NTNU

Norwegian University of
Science and Technology

CNOSSOS-EU compatible emission models for Oslo tramways and metros

Øystein Meland

Master of Science in Communication Technology
Submission date: June 2018
Supervisor: Guillaume Dutilleux, IES
Co-supervisor: Sigmund Olafsen, Brekke og Strand

Norwegian University of Science and Technology
Department of Electronic Systems

Problem Description

In this thesis we aim to create a noise emission model for Oslo metro and tram using the Common Noise Assessment Method (CNOSSOS) in EU Directive 2015/996. By using an acoustical camera we will identify the different noise sources a tram and metro train. Measurements will serve as justification for our choice of vehicle parameters in the noise assessment method. Both vehicle and track noise parameters are dependant on physical properties in CNOSSOS. As such they will be investigated and chosen according to the actual on-site conditions of the track and vehicles. By comparing the sound level from our model and measured sound level we want to further substantiate our noise emission model.

Abstract

This thesis calculates the noise emission of an metro train and tram, according to a common noise assessment method developed in the European union. To validate the choice of model parameters an acoustical camera is used to identify the position from where the noise is emitted. The accuracy of the model is found by looking at the difference between the noise emission from the calculated model, and real world measurements on trams and metro trains in Oslo. Eight measurements series of the metro train and two series of the tram were examined. Further analysis were conducted on the impact of rail corrugation on the noise emission.

The comparison between the calculated model and measurements showed us that further analysis on the model is necessary to achieve improved accuracy on the model. The thesis found room for several improvements in different aspects of the model.

Sammendrag

I denne masteroppgaven er det forsøkt å modellere lydeffekten til t-bane og trikk i Oslo. Den modellerte lydeffekten fra t-banen og trikken er basert på en beregningsmetode fra EU direktiv 2015/996. Beregningsmetoden baserer seg på at man kan finne lydeffekten til hvilket som helst tog, så lenge man kjenner til et utvalg fysiske parametere vedrørende toget og jernbanen på stedet. For å identifisere kildene og deres posisjon så har vi benytte et akustisk kamera. Våre observasjoner har fungert som verifikasjon på antagelser vi har gjort. For å bestemme nøyaktigheten til modellen sammenlignet vi målt maksimalt lydtrykk med modellert maksimalt lydtrykk. Sammenligningen baserte vi på den gjennomsnittlige differensen imellom det målte og modellerte maksimale lydtrykket i hvert 1/3 oktavbånd.

Målinger med det akustiske kameraet ble gjennomført i arbeidet med masteroppgaven. Det maksimale lydtrykket og skinnekorrugering ble målt av konsulenter hos Brekke & Strand, i samarbeid med Sporveien i 2016. Den målte skinnekorrugeringen ble benyttet til å undersøke om vi kunne oppnå økt nøyaktighet i modellen vår.

Den beste modellen oppnådde gjennomsnittlig 2.1 dB i usikkerhet i forhold til målt lydtrykk. Om man sammenlignet usikkerheten til modellen der man hadde målt skinnekorrugering og der man antok et nivå fra ISO 3095, så ser man ingen klare tegn på at den ene metoden er bedre enn den andre. Om man sammenlignet frekvensspekteret til de to modellene med målingene, så ser man at målt skinnekorrugering kan hjelpe til i å predikere topper og bunner i frekvensspekteret. Oppgaven har ett lite utvalg av målinger og flere forbedringer på modellen er foreslått om man ønsker økt nøyaktighet.

Preface

This master's thesis is the final part in my Master of Science degree in Communication technology at the Norwegian University of Science and Technology (NTNU). The project was proposed by Guillaume Dutilleux at NTNU and Sigmund Olafsen at Brekke & Strand. Brekke & Strand supplied important tools, information and data used to complete this thesis. The work presented here was conducted at Brekke & Strand Acoustics in Oslo during the spring of 2018, in cooperation with the Department of Electronic Systems at NTNU.

First of all I would thank my patient girlfriend Tirill Moseng Reiersen for loving support, and proofreading this thesis. Secondly I would like to thank my supervisor at Brekke & Strand, Sigmund, for introducing me to the world of noisy trams and subways and for making me feel utmost welcome at their office. Further I want to to express my gratitude to Guillaume at NTNU, for discussing acoustical theory and European directives with me. Finally, a thanks to my fellow student, Daniel Stusvik Haug, for helping me on my experiments.

Table of Contents

Chapter 1

Introduction

It is well established that widespread exposure to environmental noise from traffic is contributing to the disease burden in the world [1]. By creating strategic noise maps and corresponding action plans the EU wants to reduce this negative health effect throughout the European region. In the commission directive 2015/996 common noise assessment method (CNOSSOS) for strategic noise mapping according to the Environmental Noise Directive (2002/49/EC) is defined. By creating a common framework, the EU wants to create a methodical base for comparison of noise emission data between countries. This commission directive is planned to be set in effect before the 31. December 2018 in Norway. It will include noise mapping of railways with more than 30 000 train passes each year, and it will affect the metro and tram in Oslo. Currently the commission directive 2016/996 is not in full effect in Norway, as national calculation methods were allowed at the last strategic noise mapping in 2017. The Nordic Prediction Method developed in 1996 is currently being used in strategic noise mapping of the tram and metro in Oslo and Bærum. The Nordic prediction method and CNOSSOS method have different ways of defining sound power level from railways, and new key calculation parameters for both rolling stock and tracks will have to be acquired according to the Norwegian government [2]. It is stated that this input data should have accuracy of ± 2 dB [3].

This thesis aims to find key parameters for the MX3000 metro and SL-95 tram operated on the Oslo metro and tram railway network. These parameters should then be used to find the sound power level of each vehicle with the CNOSSOS method. To find the most accurate parameters we have to investigate the physical properties on the rail tracks, metro and tram vehicles. We have access to rail roughness from the last strategic noise mapping and will use this to look at if our model can be more accurate because the rail roughness parameter in CNOSSOS limits us to choose between a threshold from ISO 3095 and the average network in the Netherlands [4]. By building emission models for the metro and tram according to CNOSSOS and comparing it to already existing in-situ sound level we wish to substantiate our model. The available resources for this thesis might not be sufficient to accurately identify all aspects in the model. Therefore some assumptions will be

taken.

The key parameters for describing the rail vehicles are; the wheel roughness, aerodynamic noise, traction noise, contact filter for the wheels and transfer functions for the wheels and superstructure. The railway itself has two parameters, rail roughness and a transfer function for the type of rail. These parameters can be chosen for predefined configurations of the rolling and rail stock from a database. The database of parameters are based on analytic and empirical work done in the Harmonise project [5]. The software, TWINS, is extensively used in the CNOSSOS framework. Access and experience with it is important to develop new parameters for the description of vehicles and the transfer function for the tracks. Experimental work can alternatively be done according to ISO 3095[4]. The TWINS software is not accessible for work with this thesis, and we do not have the funds or data to do measurements according to ISO 3095. We will therefore not develop new transfer functions or vehicle specific sound emission tables. CNOSSOS defines two source lines from railway vehicles at 0.5 and 4 meters. By using a acoustical camera at out disposal we want to identify if both of these source lines are relevant for our sound power model.

Previous work on the subject of source data for CNOSSOS implementation in Nordic countries have been conducted in both Sweden and Finland and are listed here.

- [6] Report studying adjustments that have to be done in order to fit the CNOSSOS source model for traffic to Swedish conditions. Contains a study on which railway parameters that best corresponds to the current rolling and track stock in Sweden.
- [7] Paper on the work done in 2016 with the implementation of CNOSSOS in Finland. Discusses some of the problems with accuracy in CNOSSOS for Finnish conditions as little input data is known.

Chapter 2 will in this report describe sound power and propagating effects, sound attenuation and noise sources on rail vehicles. Then the details will be discussed in the emission model from CNOSSOS, and a brief introduction to the acoustical camera. Chapter 3 will explain the methodical work. With an accurate description of the rolling stock, tracks and how the measurements were conducted and what parameters were used in the modelling of the sound power. Chapter 4 shows all the results obtained from the comparison of modelled and measured sound power and their accuracy. Chapter 5 contains an analysis of the results in Chapter 4. Finally, a conclusion based on the findings and information i nthis thesis is represented in Chapter 6.

Chapter 2

Theory

This chapter will establish the theoretical basis to understand the work done in this thesis. First we will explain what sound is, and describe point source. Further aspects with the sound propagation is tied to the sound attenuation which will be discussed. Following a description of the well known noise sources on train. The last train specific theory will be regarding with how CNOSSOS models sound power from trains and its propagation model. The theory chapter also contains a short description of the acoustical camera used in this thesis.

2.1 Sound

Sound can be described as the movement of acoustic waves within the frequency range of the human ear [8]. Acoustic waves are emitted from mechanical devices that vibrate and alter the ambient atmospheric pressure [8][9]. Sound pressure *p* will change in space *x* and time *t*. How it changes depends on the source and what type of wave it emits, these can be plane, geometrical or other wave types. When looking at these sources we want to use the root mean square value *rms* of the pressure since the pressure amplitude can be both positive and negative.

$$p_{rms}^2 = \frac{1}{T}\int_0^T p^2(t)dt \tag{2.1}$$

This can further be used to find the sound pressure level L_p with a commonly used reference value p_0 for air that is $20\mu Pa$

$$L_p = 10\log_{10}(\frac{p_{rms}^2}{p_0^2}) \tag{2.2}$$

L_p is expressed in *decibel* and is a useful scale for us humans to understand. The human ear can approximately comprehend signals between 0 to 140 decibels. The smallest audible change between two pressures match 1 dB. 10 dB increase is the same as one doubling of the stimulus to the ear.

The *sound power* is a dimensionless description of the total sound pressure exerted from a source, and can be written like this

$$W = \rho_0 c_0 S \overline{v^2} \sigma \tag{2.3}$$

where S will be the surface area of the source, $\overline{v^2}$ is the squared velocity normal to the surface which is averaged over time over the surface area, c_0 that is the speed of sound in air and the σ is the *radiation ratio*. This is the ratio of the sound power emitted in the real world compared to what would be an ideal source radiation of plane waves. The radiation ratio is calculated from the size and shape of the source.

The point source is a pulsating sphere where the radius *r* varies over time giving the radial surface velocity of $u = \hat{u}e^{jwt}$.

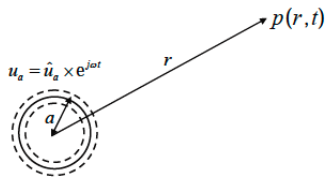

Figure 2.1: Point source.[10])

If the sphere is compact i.e. $a << \lambda$, the excursion ϵ will be $\epsilon << a$ of the sphere and the medium surrounding the sphere is infinte, homogeneous and isotropic, then the sphere will radiate a spherical wave outward that is well defined from [8, 9, 10, 11] with wavenumber $k = 2\pi/\lambda$.

$$p(r,t) = \frac{\rho_0 ck}{4\pi r}|u(a)|e^{j(wt-kr)} \tag{2.4}$$

The directivity $D(\theta, \phi)$ is a description of the beam pattern from a source. For the compact spherical source radiating with power W into free space the mean square sound pressure will be

$$p^2 = \frac{\rho_0 c_0 W}{4\pi r^2} D(\theta, \phi) \tag{2.5}$$

where θ is the elevation and ϕ is the azimuth of the receiver related to the source. The directivity factor can be defined from an expression like $D = 2cos^2\theta$ for the oscillating cylinder. For a omni directional source the directivity factor is simply 1.

When a sound source is positioned close to the ground we have to take the sound reflection into account. The sound reflection acts like a mirror source as in figure (2.2). We denote the sound source with S, sound power P and the mirror source with S'. The ground will have a sound absorption factor α_{ground} and reflection factor $\rho_{ground} = 1 - \alpha_{ground}$, giving us the factor for the mirror source ρ_{ground}. [9].

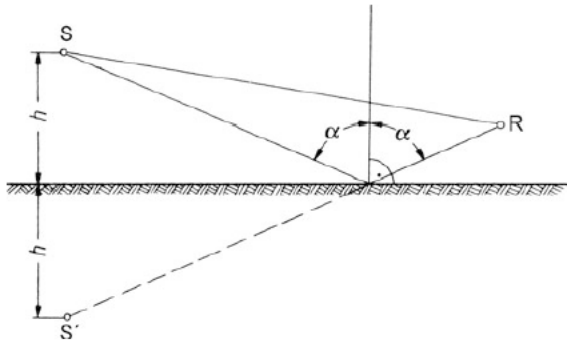

Figure 2.2: Ground reflection from source S above horizontal plane [9]

2.2 Sound attenuation

2.2.1 Geometric attenuation

The attenuation due to geometrical divergence occurs due to the energy conservation as a wave spreads out from a source. It is independent of frequency and it describes the loss of sound pressure due to the reduction of sound power as the area of one geometry increases. One important surface for consideration is the sphere. The intensity I of the omni directional sphere is described by

$$I = \frac{W}{4\pi r^2} \tag{2.6}$$

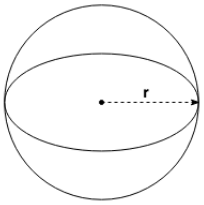

Figure 2.3: Cylinder

If the distance **r** is large enough, the wave can be approximated to a plane wave [8], then the intensity equals

$$I = \frac{p_{rms}^2}{\rho_0 c_0} \tag{2.7}$$

giving us the sound pressure

$$p_{rms}^2 = \frac{W \rho_0 c}{4\pi r^2} \tag{2.8}$$

With the conversion constant from the relationship between sound pressure and sound power on 1 meter distance we get the dB value for the geometrical divergence from a sphere.

$$A_{sphere} = 20\log_{10}(\frac{r}{r_0}) + 11 \tag{2.9}$$

where r_0 is a reference distance of 1m.

2.2.2 Atmospheric attenuation

When the sound propagates through the air, some of the energy is absorbed by the thermal conductivity and viscosity of the air. In addition we have the molecular absorption from the relaxation between the air molecules which is also included in the atmospheric attenuation. The attenuation is dependant on the humidity and frequency, and is reduced proportional to the distance the sound travels. In this thesis none of the sound propagation paths will exceed 16m, as such the atmospheric attenuation will be negligible for the models use [9].

2.3 Noise sources on rail vehicles

The sound from a train can be divided into two different types of sound sources with distinct properties [11]:

- Structural vibrations - The vibration of a structure cause movement of surrounding air particles which produces sound, i.e on a train the wheel or engine, but it can also be the rail it travels on.

- Unsteady aerodynamic flow - From turbulence cause by air flowing past structures or air flowing out from pipes or holes. On a train this could be the pantograph or exhaust port.

Three distinct dominant noise groups can be identified at different speed ranges; engine noise, rolling noise and aerodynamic noise. The engine noise is mainly dependant on the type of train. Typically an electric passenger train will have lower engine noise than a diesel electric train. The rolling noise originates from the contact point between the rail and wheel of the train, and is dependant on the roughness of them both. And the aerodynamic flow that appears as trains pass 200 km/h [5].

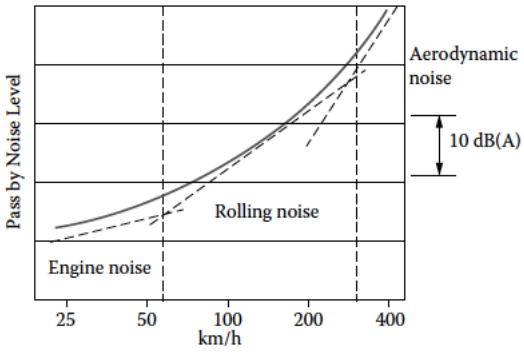

Figure 2.4: Pass by noise level from dominant sources at different speed ranges [5]

2.3.1 Rolling Noise

The noise from the wheels and tracks is defined as rolling noise. The noise originates from the contact point between them, the rail and the wheel structure. The cause of the noise is the surface irregularities on both the rail and wheels. The surface irregularities are defined as the roughness of the surface, that is the rail roughness and the wheel roughness. The roughness creates vertical dynamic forces which results in vibrations of the rail and wheel. The excited surfaces of the wheel and track amplifies the vibrations and create noise. Both the rail and wheel roughness can vary in wavelength, and subsequently amplify the noise stronger at corresponding wavelengths. The typical wavelength range that excites noise from the wheel and rails is between 5 to 500mm. If a wavelength is present on the track with a train moving over it, it will create a sinusoidal vibration with a frequency [11].

$$f_{vibration} = \frac{v_{Train}}{\lambda_{Track}} \tag{2.10}$$

Over time, the continuous wear from the rolling stock will wear down the track and increase its roughness. There is no consensus about what causes the deterioration of the track [5], but a common assumption is that that breaking, acceleration, the type of wheel and its condition are the main origins. To prevent excessive roughness on the railway, grinding of the track can be executed. If the roughness of the wheels are high, they will excite larger vibrations which could lead to faster increasing roughness levels. As will large roughness levels of the track increase the deterioration of the track itself when trains travel on it.

Figure 2.5: Rail corrugation on rail on one part of the metro tracks in Oslo [12]

The roughness level L_r is a measure of the roughness on the wheel or track. With the mean square value of the vertical displacement difference of the contact surface to the mean level represented as r with a reference r_0 of $1\mu m$.

$$L_r = 10\log_{10}(\frac{r}{r_0})^2 \tag{2.11}$$

The roughness level can span a spectrum of wavelength λ. As a result the frequency spectrum of the roughness level will shift at different speed according to equation (2.9).

2.3.2 Engine Noise

Engine noise modelling is different than rolling noise modelling, because of large variations of train designs. Between electric and diesel driven trains the engine itself is completely different. The exhaust from a diesel engine is an example of a strong noise source, and it can be positioned at different heights on every train. From electric trains the engine noise and the drive train itself is often the strongest sources. Both electric and diesel trains use fans for cooling of different parts. And depending on the design of the train the fans can be positioned anywhere.

2.3.3 Aerodynamic Noise

On trains the aerodynamic noise can come from multiple positions, mainly the pantograph and the bottom part and around the boogies. It can also originate from the whole train itself, at high speeds. Aerodynamic noise from trains is not important when the train is moving slower than 160 km/h [9, 11, 13, 14]. In this report we look at trains and trams moving at maxiumum 70 km/h and therefore aerodynamic noise will not be taken into consideration.

As such it will not be taken into consideration further in this report, since we are looking at trains and trams moving at maximum 70 km/h.

2.3.4 Other distinct sources

In addition to the previously discussed noise sources we have these uncategorized sources.

- *Impact noise* occurs when a train passes gaps on the track. This can be rail joints, crossings or switches. The strength of the noise varies depending on shape of the gap, its shape and at what speed the train pass it.

- *Curve squeal* is found where the rail curves. The squeals magnitude is dependant on curvature, friction, speed of the train, track-wheel geometry and dynamics.

- Other structural radiations from bridges, viaducts and tunnel openings can amplify the noise. A bridge can be set in motion of the train and act as a larger radiating surface. And a tunnel opening can amplify the noise as a trumpet.

2.4 CNOSSOS model

On the 19th of may in 2015 the European Union implemented the commission directive for establishing a common noise assessment method according to Directive 2002/49/EC of the European Parliament and of the Council. This directive contain a method for mapping noise, to be used to avoid, prevent or reduce the harmful effects of noise. The method is the result of a project begun in 2008 which aimed to make one common method for noise mapping. The requirement to make a common method occurred because of difficulties when multiple nations or regions had their own calculation methods [13]. The CNOSSOS method is based on the work from the Harmonise, NMPB and Nord2000 projects. As this thesis is looking at the source description of the metro train, only the rail method will be described here. For further insight, the reader is encouraged to read the document itself. That can be found on the EU-parliaments homepage.

2.4.1 Sound Power

In CNOSSOS a train is defined as multiple connected sub vehicles, where each vehicle can be independent in itself, that is a locomotive, self propelled coach or freight coach[13]. Table 6.1 in the Appendix show the common classifications and descriptors of different railway vehicles. Each of these descriptors are intended to be used when we want to define the sound power spectra from different parts of the vehicle. And from the different sound power spectrum we can calculate the sound power per vehicle

Rails and support components and their acoustical properties will vary throughout railway networks. From rough tracks on wooden sleepers, to well maintained continuously welded rails with noise mitigating measures. The most important descriptors for the track is the track base, rail head roughness, rail pad type, additional measures, rail joints and the curvature. The railway has to be divided into track sections with descriptors from table 6.2 that reflect the on site properties.

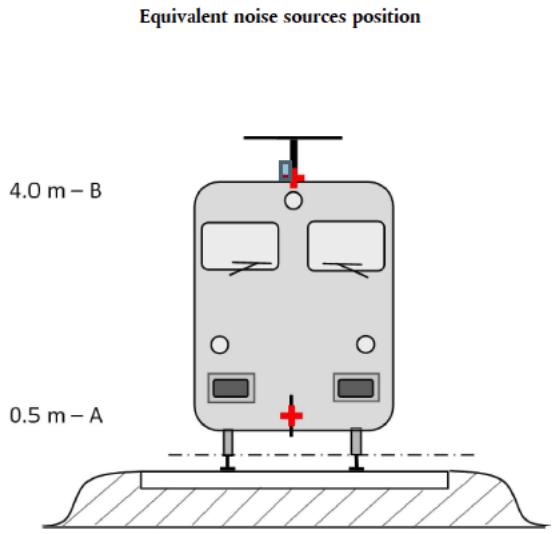

Figure 2.6: Noise source positions on a train as defined in [13]

The source lines on the trains are defined at the centre of the track and at 0.5 and 4.0 meters above the railhead as in figure 2.6. At these two lines, the noise sources are divided according to different categories. On position A at 0.5 we have the following contributing sources.

- Rolling noise that consists of multiple contributions, i.e the roughness of the wheels and rail, the contribution from the track and its surfaces.
- Traction or Engine noise that comes from the drive-train, electric motors, gears, fans or diesel engine blocks.
- Aerodynamic noise from shrouds and screens on the bogies.
- Impact, Squeal and Bridge noise

For position B the following source are defined.

- Aerodynamic noise from the pantograph.
- Traction noise from fans, exhaust and cooling outlets positioned at the roof.

The rolling noise is modelled from multiple elements; wheel roughness, rail roughness, vehicle transfer function and track transfer function. For wavelengths between 0.8 to 1000mm we can find values for these parameters depending on the condition of the track, wheels and type of brakes. The values can be looked up in tables, and we believe that they are based on measurements on European rail vehicles and tracks [6]. Wheel and roughness have been discussed already, but the transfer functions have not. They are included to be able to decouple the trains and tracks. The transfer functions are supposed to represent

the mechanical vibration and sound generation on the surfaces on the whole system of wheels, rails and support. Three important elements are used to find the total and effective roughness level $L_{R,TOT,i}$.

$$L_{R,TOT,i} = 10\log_{10}\left(10^{L_{r,TR,i}/10} + 10^{L_{r,VEH,i}/10}\right) + A_{3,i} \tag{2.12}$$

- The rail roughness level $L_{r,TR,i}$, that is assumed to be in a certain condition in table 6.3, or that can be measured.
- The wheel roughness level $L_{r,VEH,i}$, which is the eqvivalent to the rail counterpart but for wheels found in table 6.4.
- The contact filter $A_{3,i}$, that considers filtering in the contact point between track and wheel found in table 6.5.

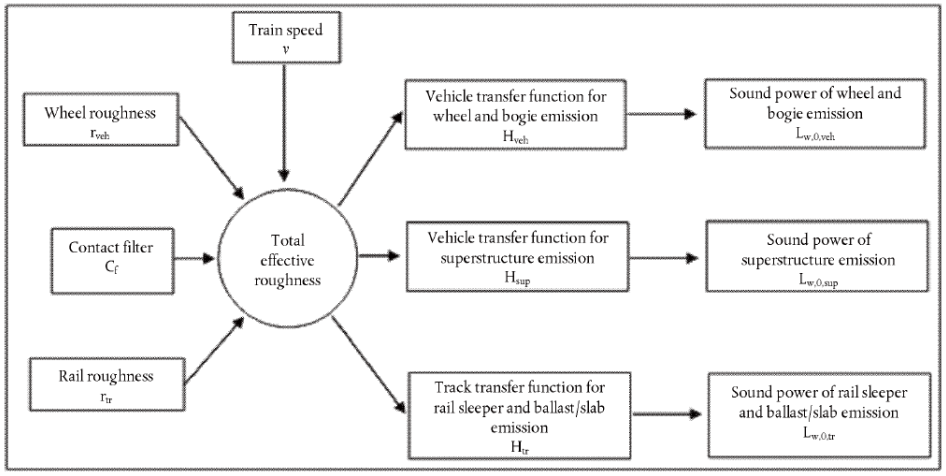

Figure 2.7: Scheme from CNOSSOS to use roughness and transfer functions to find sound power [13]

The transfer functions are denoted $L_{H,TR,i}$, $L_{H,VEH,i}$ and $L_{H,VEH,SUP,i}$. They are used to combine the total effective roughness level $L_{R,TOT,i}$ with the sound power from the track, wheels, superstructure and number of axles N_a to find the sound power per vehicle. Freight trains are not discussed in this thesis and therefore we will not include the superstructure transfer function.

$$L_{W,0,TR,i} = L_{R,TOT,i} + L_{H,TR,i} + 10\log_{10}(N_a) \tag{2.13}$$

$$L_{W,0,VEH,i} = L_{R,TOT,i} + L_{H,VEH,i} + 10\log_{10} log(N_a) \tag{2.14}$$

The engine noise is modelled in two operating conditions, when moving at constant speed and idling for more than 30 min. These two conditions have the same source strength giving us $L_{W,0,const,i} = L_{W,0,idling,i}$, because the CNOSSOS method only models the

engine noise when the train is at maximum load. Depending on the train type descriptor in 6.1 we can look up the engine noise spectrum in table 6.8. It is possible to measure the whole train or each individual source to retrieve the values in this table. To measure the whole train ISO 3095:2013 should be used. The sound power distribution between position A and B should be done according to where the noise sources are positioned for each specific vehicle.

The squeal effect is considered for curves with radius below 500 meters and where the curve section is at least 50 meters long. When the radius is between $300 < R < 500$, then 5 dB should be added for all frequencies. If the radius is $R < 300m$ then 8 dB shall be added. CNOSSOS states that normally this should be verified on site, and especially for trams.

The horizontal directivity is defined in the horizontal plane and is assumed to be dipole given for each frequency band *i*:

$$\Delta L_{W,dir,hor,i} = 10\log_{10}(0.01 + 0.99\sin^2\varphi) \tag{2.15}$$

The vertical directivity is given by two functions according to if it is from position A or B. In position A the directivity is defined in the vertical plane for each frequency band *i* and for $-\pi/2 < \Psi < \pi/2$.

$$\Delta L_{W,dir,ver,i} = \left(\left|\frac{40}{3}\left[\frac{2}{3}\sin(2\Psi) - \sin(\Psi)\right]\log_{10}\left(\frac{f_{c,i}+600}{200}\right)\right|\right) \tag{2.16}$$

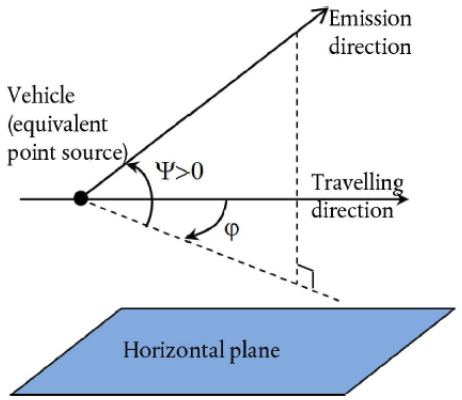

Figure 2.8: Figure of horizontal and vertical directivity [13]

In position B the source sound power is modelled as

$$\Delta L_{W,dir,ver,i} = 10\log_{10}(\cos^2\Psi) \tag{2.17}$$

Impact noise is included in the rolling noise term in CNOSSOS. But in this thesis we will, for simplicity, avoid crossings, switches and junctions on the rail. Aerodynamic noise is only to be included if the trains move at speeds above 200km/h, and the maximum speed of our trains are 70km/h. Other noise contributing elements that are not included are structural radiation from bridges and viaducts.

The sound power from each vehicle are obtained from energetically adding the sound power level from each source **j** (rolling, impact, squeal, engine, aerodynamic and other effects) in each 1/3 octave band.

$$L_{W,0} = 10\log_{10}\left(\sum_j 10^{\frac{L_{W,0,j}}{10}}\right) \tag{2.18}$$

When all the acoustic noise parameters of the rail section has been defined, the directional sound power per vehicle can be found.

$$L_{W,0,dir,vehicle} = L_{W,0} + \Delta L_{W,dir,vert} + \Delta L_{W,dir,hor} \tag{2.19}$$

To find the directional sound power per axle we use the following equation.

$$L_{W,0,dir,axle} = L_{W,0} + \Delta L_{W,dir,vert} + \Delta L_{W,dir,hor} - 10\log_{10}(N_a) \tag{2.20}$$

2.4.2 Sound propagation

CNOSSOS have the following method for modelling sound propagation, and we will explain the important aspects for our implementation. The sound level L_H in homogeneous conditions is defined by

$$L_H = L_{W,0} - A_{Sphere} - A_{Atm} - A_{Boundary} \tag{2.21}$$

$L_{W,0}$ is the sound power of the source, A_{Sphere} from equation 2.12, atmospheric attenuation A_{Atm} and $A_{Boundry}$ which contains other effects such as

- A_{ground} which is the ground absorption or reflection.
- A_{dif} that is the attenuation due to diffraction.

The propagation path in CNOSSOS is defined over a mean ground plane between the source and receiver if $A_{boundary} = A_{ground}$. The equivalent height of the source z_s and receiver z_r is orthogonal to the mean plane. We do not know the on-site topography, so z_s is assumed to be on the height of source A on the train, and z_r is assumed to be equal to the height of the microphone when measured.

2.4.3 Ground effect

We will calculate A_{ground} with no diffraction, which means $A_{boundary} = A_{ground}$. The ground effect in CNOSSOS is a combination of the interference that occurs due to the

reflection from the ground, and the sound that propagates directly. To determine the attenuation we have to establish some values. The distance between the source and receiver is defined as $d_p = \sum_i d_i$ where d_i is each sub path over different type of ground. The ground factor G_{path} is defined as $G_{path} = \frac{\sum_i G_i d_i}{dp}$ where G_i is the ground factor at the corresponding sub path d_i. The acoustic absorption from the ground is represented by a value G that varies from 1 to 0. Where 1 is strongly absorbent and 0 is almost perfectly reflective. When the distance is small between the source and receiver according to

$$d_p \leq 30(z_s + z_r) \tag{2.22}$$

the distinction between the ground factor at the receiver and source is negligible. With a corrected equation for the ground factor G_{path}

$$G'_{path} = \begin{cases} G_{path}\frac{d_p}{30(z_s+z_r)} + G_s\left(1 - \frac{d_p}{30(z_s+z_r)}\right) & \text{if} \quad d_p \leq 30(z_s + z_r) \\ G_{path} & \text{otherwise} \end{cases} \tag{2.23}$$

Then we can calculate the attenuation with the following equation, as long as $G_{path} \neq 0$.

$$A_{Ground} = max\left(-10\log_{10}\left[4\frac{k^2}{d_p^2}\left(z_s^2 - \sqrt{\frac{2C_f}{k}}z_s + \frac{C_f}{k}\right)\left(z_r^2 - \sqrt{\frac{2C_f}{k}}z_r + \frac{C_f}{k}\right)\right], A_{Ground,min}\right) \tag{2.24}$$

C_f and w are given by the following equations

$$C_f = d_p\frac{1 + 3wd_pe^{-\sqrt{wd_p}}}{1 + wd_p} \tag{2.25}$$

and

$$w = 0.0185\frac{f^{2.5}G'^{2.6}_{Path}}{f^{1.5}G'^{2.6}_{Path} + 1.3 \cdot 10^3 f^{0.75}G'^{1.3}_{Path} + 1.16 \cdot 10^6} \tag{2.26}$$

where f is the 1/3 octave band frequency. $A_{Ground,min}$ is the lower bound given by equation

$$A_{Ground,min} = -3(1 - G_{path}) \tag{2.27}$$

2.5 Acoustic Camera

An acoustic camera is a array of microphones positioned in a system, such that signal processing techniques can be applied to identify sound sources. By combining the camera and the microphone array, it is possible to visually identify these sources. The shape, size, density of microphones and their distribution are important parameters in determining the efficiency of the array. Theoretical aspects of the acoustic camera will not be explained in detail since it is only used as a measurement tool. However, by looking at the technical notes from Norsonic we can get some insight into how the acoustic camera performs. In

figure 2.9 we can observe the density and distribution of microphones and the beam pattern of the array.

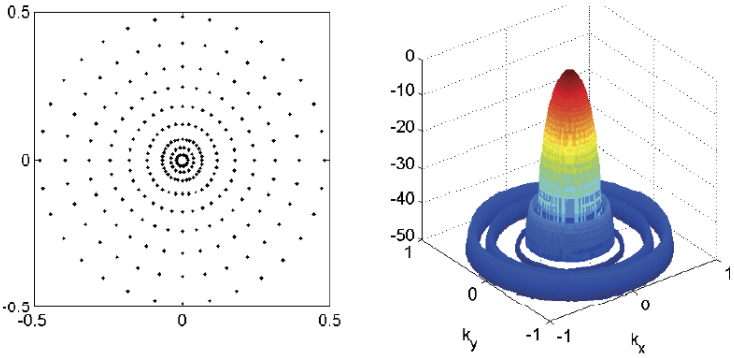

Figure 2.9: Norsonic 848A-10 beam pattern [15]. The size of the array is from -0.5m to 0.5m and the beam pattern strength is normalised and in dB.

We can see from the beam plot that the circular blue side lobes are small compared to the large red main lobe. This is important for the acoustic camera ability to distinguish between real sources, sources that do not exist and interfering signals. With a large difference between the main lobe and side lobe, the camera will be able to suppress these sources [16]. The distinct pattern of the beam is due to the array design in the left plot in figure 2.9. In short, the high amount of microphones in an increasing density from the edge to the centre creates this pattern, combined with signal processing techniques. With a diameter of 1 m it makes a accurate array for our measurements.

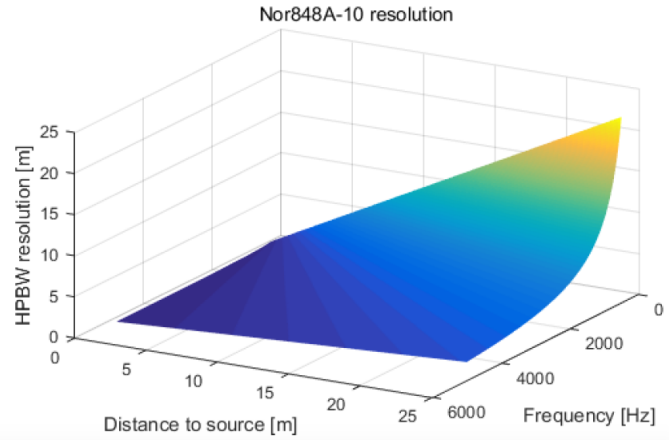

Figure 2.10: Norsonic 848A-10 resolution [17]

The resolution of the acoustic camera determines how far sources have to be from each other in order to identify them. This is related to the performance of the camera, but

also what frequency the sources transmit and at what distance. The resolution is plotted in figure 2.10 with regards to distance from the receiver and frequency transmitted. The resolution is defined in [m] and calculated from the half main lobe width [17]. We immediately see that resolution is good for all frequencies when the array is close to the source below 5m, but when the distance increase the resolution is reduced for the lower part of the spectrum. That tells us that the best performance comes from a large array when it is close to the sources.

Chapter 3

Methodology

This chapter will at first list the equipment used in this thesis. Then we will look at a through description of the rail and rolling stock of the metro network under study. Further we will present how the measurements were conducted, and where they were executed. A thorough description of how the model were implemented is also described. Next we will look at a comparison between our model and measurement. Finally we will present measurements series conducted by Brekke & Strand at each geographical position with both ingoing and outgoing track.

3.1 Equipment

- Norsonic Acoustical Camera Nor848A-10
- Norsonic Power cable - Nor4574
- FirstPower Rechargeable battery - FP 1270
- Apple MacBook Pro 15 inch 2017 (Required acoustical camera)
- APT - Rail surface analyser
- Norsonic Sound Analyser - Nor140
- Norsonic Sound Analyser - Nor121

3.2 Rail and Rolling stock

In this section we want to describe the rail and rolling stock and find suitable descriptors according to the CNOSSOS method. Kolsåsbanen railway was rebuilt between 2009 and 2014 from Bjørnsletta to Kolsås station. Both the metro train MX3000 and tram SL95 run on theses tracks. Due to the tight curvatures on the rail path, the maximum speed is

limited to 50 km/h for both the tram and metro. Preventive rail grinding is performed on the whole railway network in Oslo, and the last grinding of this part of the track was done in 2015. All characteristics to the railway stock is equal for all the geographical positions examined in this thesis.

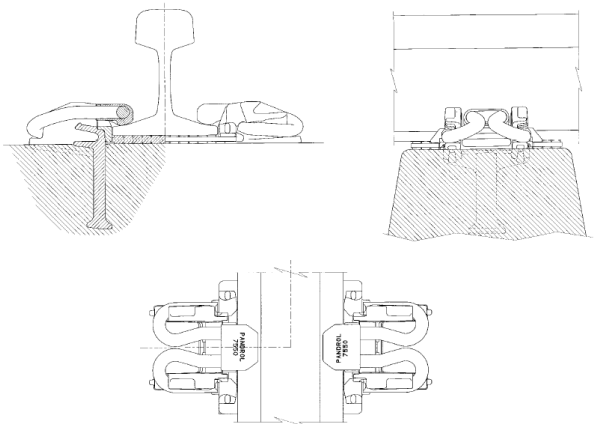

Figure 3.1: Schematic of track construction [18]

On the schematic in picture 3.1 we can see how the railway track on Kolsåsbanen is built. In the CNOSSOS method the base, pad type and additional measures are used to calculate the sound power level of the track. The track base is of the **Ballast** type with rough gravel as we can see in figure 3.2.

Figure 3.2: Part of 49E1 rail track with JBV 97 sleeper and gravel base.

The dynamic stiffness of the assembly FC1501 is 80-280 MN/m and the static stiffness is 70-210 MN/m [19]. Based on this we will give the assembly the descriptor code **Soft** which ranges from 150-250 MN/m. The rails are continuously welded on the part of the track under examination, so the rail joint descriptor is **None**. Concerning the curve squeal this will not be included in our model, as CNOSSOS recommends on-site verification. There are no additional noise reduction measures on the parts of the track we picked, giving the code **None**. The last important track descriptor is the rail roughness. This can be measured or assumed from a default set of values: **Well maintained, Normally maintained, Not well maintained, Not well maintained and bad condition**. We will use the measured rail roughness level and compare it to the **Well maintained** descriptor.

Table 3.1: Track components from [18]

Rail stock				
Rails	Clips	Toe/Side isolator	Pad	Sleeper
49E1	Pandrol FC 1501	Sk 3162a/Sk 3163	Sk 3166 (10 mm)	JBV 97

There are two types of trains that run on the sections that will be examined, the metro train MX3000 and the tram SL-95. From figure 6.1 we can read that this gives us vehicle type **c** for **city tram or light metro self-propelled and non-self-propelled coach**. MX3000 were set in use in 2007 and replaced the old T1000 and T1300 stock while the SL-95 replaced the SL-79 on sections of the network. The metro train are built together in 3 cars per unit, with 2 units in a train. It is able to run at maximum 80 km/h, but due to the sharp curves throughout the metro network in Oslo, the maximum speed limit is set at 70 km/h, and it will only achieve such speeds at the end of the night shift with no passengers.

Figure 3.3: MX3000 boogie with visable brake disks and traction motor.

Other important characteristics are the power lines which run along the track about 0.5 m above the ground. The traction unit is positioned inside the boogie of each car [20]. The brake system consists of multiple types of brake, two disk brakes on each axle, rail brakes when the train is at standstill and regenerative magnetic brakes. Giving the MX3000 descriptor for brakes as **n** for **non-tread braked, like disc, drum and magnetic brakes**. Each vehicle has 4 axles, with a total of **12** axles on one MX3000 unit. No other noise reduction equipment is present, giving **n**, **no measure**. The remaining important descriptors of the MX3000 unit is listed in table 3.2

Table 3.2: MX3000, three car train technical data [20].

Length	Width	Tare Weight / Total Weight	Max Speed	Axle Load	Wheel diameter new/worn
54,340 mm	3,160 mm	94 t / 141.5 t	80 km/h	12.5 t	850 / 770 mm

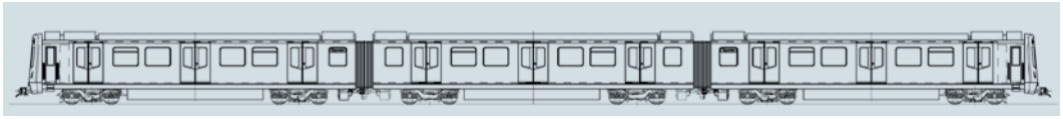

Figure 3.4: MX3000 [20]

The SL-95 tram is based on 3 vehicles where the first and third is larger than the second vehicle. The middle vehicle has 4 axles while the others have 2 axles each. SL-95 is substantially heavier at 80 tons compared to its predecessor SL-79. The tram has 2 disc brakes at each axle. The traction equipment is positioned low on the vehicles around the boogies.

Table 3.3: SL-95 technical data [21].

Length	Width	Tare Weight / Total Weight	Max Speed	Axle Load	Wheel diameter new/worn
33,120 mm	2,600 mm	65 t / 80 t	80 km/h	10 t	680 / 610 mm

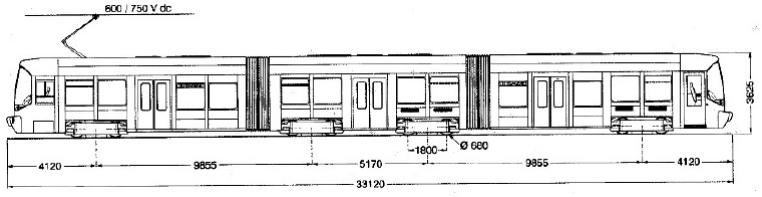

Figure 3.5: SL-95 [22]

3.3 Field measurements

3.3.1 Determining noise source positions

To model the noise from the metro train and tram we have to know where the different noise sources are positioned and their approximate strength. With the acoustical camera we can make accurate measurements of both noise position and strength. The acoustical cameras ability to pin point the low frequency noise sources depends strongly on the distance between the source and camera. That is why we wanted to position the camera as close as practically possible to the railway.

(a) Norsonic Nor848A-10

(b) Pass by measurement with acoustic camera of SL95 tram

Figure 3.6: Acoustic Camera

Table 3.4: Technical specifications of Norsonic Nor848A-10 Acoustical Camera [23]

Nor848A-10				
Number of microphones	Mapping frequency range	Self noise	Operating Range	Analysing Spectrum
256	125-15kHz	9 dB[A]	0.5m - 200m	1/1 and 1/3 octave

We positioned the acoustical camera at the side of the track at axle height and approximately around 4m relative to the track, to identify all the sources on the tram and metro. In figure 3.7 we can see a screenshot of the acoustical camera software. On the left side we can see the sound pressure level range. The bottom slider defines the frequency range, we chose a frequency range from 63 Hz to 20kHz. The coloured circles indicate the strongest source measured according to the decibel range and frequency range set by the user. All the measurements were done with unweighted and fast response of 125ms.

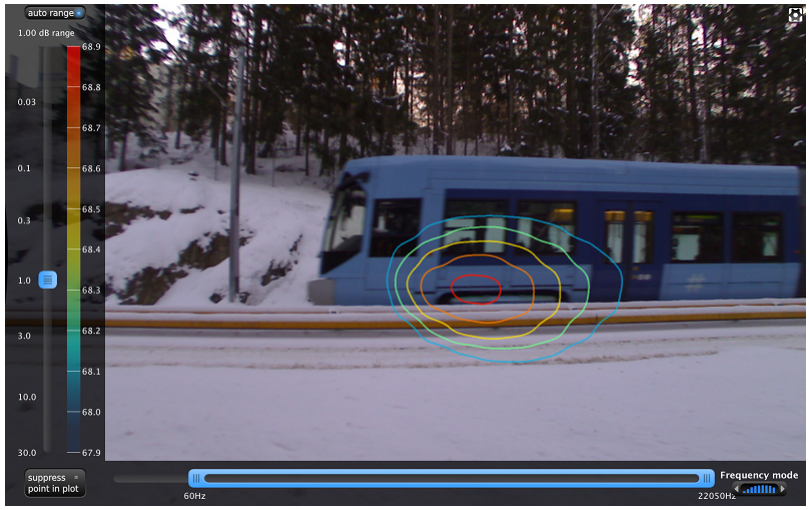

Figure 3.7: Screenshot of Norsonic software used with acoustical camera measuring a SL-95 tram.

3.3.2 Measurement of rail roughness

Noise exposure has been measured on multiple positions on the metro network in Oslo as a part of the noise monitoring program from Sporveien, simultaneously as the rail roughness has been measured. The noise monitoring program for the tram began in 2007, and for the Metro it began in 2016. The measurements have been conducted by Brekke & Strand acoustics according to ISO 3095, each year on 11 different positions.

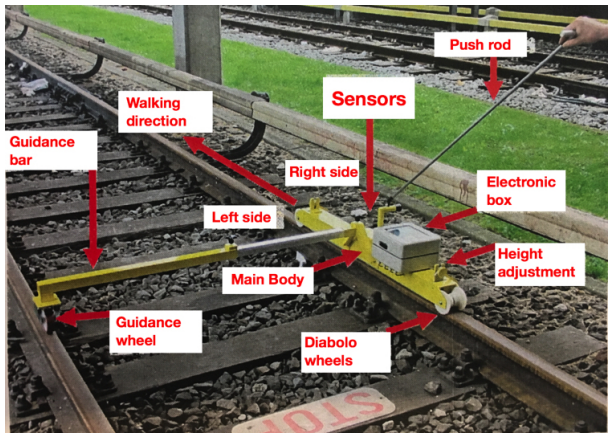

Figure 3.8: APT - Rail Surface Analyser

The measurements were performed with a rail surface analyser from APT. By pushing the RSA in 3.8 three displacement sensors as seen in 3.9 senses the vertical distance with the sliding beam as a reference point. The walking speed of the operator were not higher

than 1m/s as this is the maximum operating speed for the RSA. The sliding beam is 1 m long, giving the RSA the ability to measure wavelengths from 4mm to 500m. The system noise floor is $\pm 0.03 \mu m$ for a measurement range of 5mm. The limitation of how long sections of the railway that can be measured depends on the internal memory, or if the roughness pattern exceeds the vertical displacement limits. As the RSA does not measure the rail roughness level from 1000mm to 0.8 mm we synthesised the missing wavelengths with interpolation in Matlab.

Figure 3.9: Three displacement sensors on the rail side of the rail surface analyser.

When measurements have been completed its possible to extract a roughness spectrum as shown in figure 3.10.

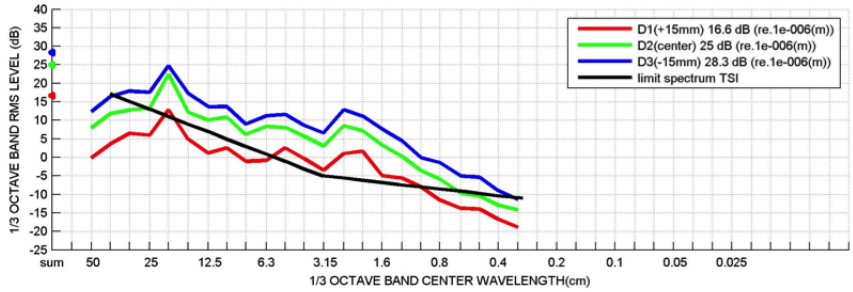

Figure 3.10: Typical spectral data from a rail roughness measurement with three different sensors D1,D2 ad D3

3.3.3 Position of measurements

The pass by sound pressure levels were measured on 4 different geographical locations; Dalbakkveien, Linderudveien, Åsjordet and Tjernsrud Plass. Only Tjernsrud plass had both tram and metro running on the same track.

Table 3.5: Coordinates for the positions where measurements were conducted

Dalbakkveien	Linderudveien
59°54’11.2”N 10°5450’11.8”E	59°56’32.4”N 10°50’32.7”E
Åsjordet	Tjernsrud plass
59°55’40.9”N 10°38’36.7”E	59°55’14.7”N 10°36’37.3”E

Figure 3.11: Measurement position at Dalbakkveien.

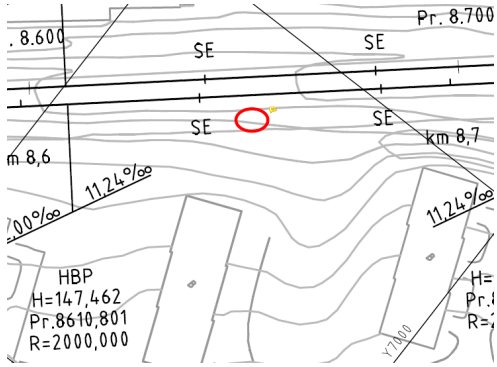

Figure 3.12: Measurement position at Linderudveien.

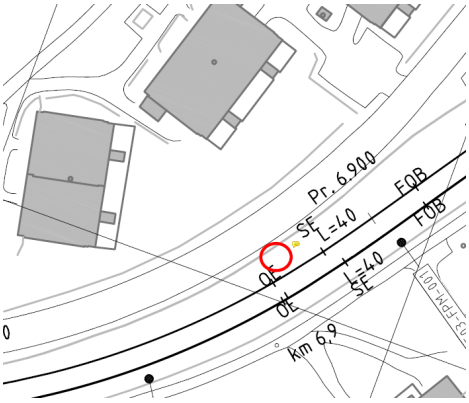

Figure 3.13: Measurement position at Åsjordet.

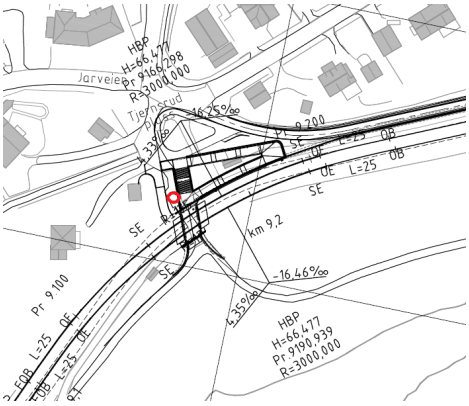

Figure 3.14: Measurement position at Tjernsrud plass.

The position of the microphone used in the measurements are sketched in figure 3.15, and a table with their values are shown in table 3.6. Different amount of passes were measured on each position, as their time tables are different and the consultants only had a predefined time limit at each place. One Norsonic 140 were used to measure both equivalent and maximum sound level. The speed of the passing vehicles were received from measuring the average pass by time. The average pass by time and frequency of passes are listed in table 3.7

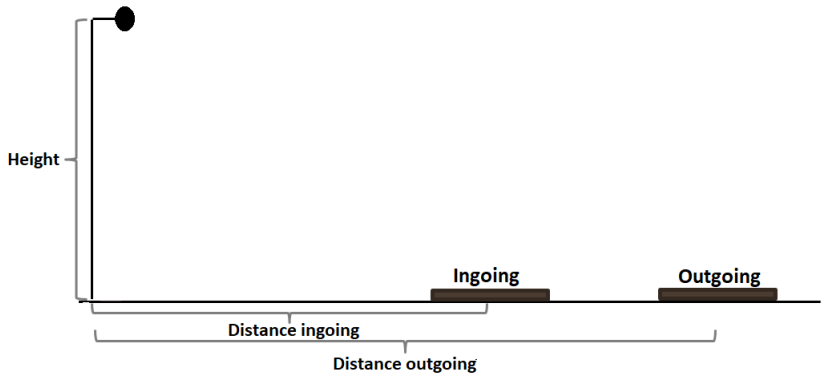

Figure 3.15: Measurement position of microphone.

Table 3.6: Measurement setup on each location.

	Distance outgoing [m]	Distance ingoing [m]	Height [m]
Dalbakkveien	4.5	9.0	2.0
Linderudveien	11.5	16.5	1.7
Åsjordet	9.1	4.6	2.0
Tjernsrud plass	10.0	5.5	2.0

Table 3.7: Average speed and number of passes of trains on location

	Average speed [km/h]		Number of Passes	
	Outgoing	Ingoing	Outgoing	Ingoing
Dalbakkveien	33	43	12	9
Linderudveien	61	57	4	3
Åsjordet	46	48	10	10
Tjernsrud plass	47	46	10	10
Tram at Tjernsrud plass	46	45	6	6

3.4 Modelling the sound power level with the CNOSSOS method

As discussed in chapter 2 the CNOSSOS method for estimating the sound power level from trains is based on the total effective roughness level and corresponding transfer functions. In this section we want to go through how we choose the different transfer functions and how they were used to determine the sound power levels. We will describe how we calculated the sound power from the parameters describing the track and vehicles with the CNOSSOS software.

Table 3.8: Overview of CNOSSOS modelling parameters

Coefficients	**MX3000**	**SL-95**
$L_{R,Vehicle}$	Disk Brake	Disk Brake
$L_{R,Track}$	Measured	Measured
A_3	25kN - 920mm	50kN - 680mm
$L_{H,Track}$	Mono block sleeper soft rail pad	Mono block sleeper soft rail pad
$L_{H,Vehicle}$	840mm wheel diameter	680mm wheel diameter

The total effective roughness level defined in chapter 2.5, is based on the train speed, wheel roughness level, rail roughness level and a contact filter. Both the tram and metro uses regenerative brakes in combination with disc brakes. Regenerative brakes are not stated as an option in table 6.4 reproduced from CNOSSOS. But as we can see in figure 3.3 the boogie has 4 disk brakes. The choice of brakes will influence the rolling noise as it describes how the wheels are worn and how they sound when decelerating. Breaking pads will for example wear down the wheels unevenly. There are limited options for choosing the contact filter coefficients, but we tried to pick the one with the least deviation from the actual axle load and wheel diameter. The weight is not as influential on the contact filter [4] as the diameter, as such the diameter was chosen first, secondly the axle load. As we can see in figure 3.2 the sleeper is a mono concrete block, and as stated previously, the pad type is considered soft. Both the tram and metro run on the same track and they have the same track transfer function. The transfer function for the vehicles is however different, decided by the wheel diameters.

In the process of making CNOSSOS a source model software has been developed. It uses XML files, containing vehicle and track parameters to calculate equivalent sound power level according to the equations stated in the theory section of this thesis. The software is manipulated with four different XML files: CNOSSOS_Rail_Input, CNOSSOS_Rail_Output, CNOSSOS_Rail_Track and CNOSSOS_Rail_Vehicle. The input files defines what kind of scenario should be modelled, and all the relevant parameters are listed in table 3.9.

Table 3.9: Additional parameters used in CNOSSOS source model software to model sound power level from MX3000 metro and SL-95 tram

Section length (MX3000/SL-95)	Horizontal/ Vertical angle	Curve radius	Running condition	Speed	Source position
54 / 33	90 / 0	Straight	Constant	Average speed measured on-site	A

The section length was chosen according to the length of the tram and metro. The horizontal angle was chosen to be 90 degrees and the vertical angle at 0, because sound pressure levels were measured perpendicular to the rail track. The radius of the curvature was decided in section 3.2. At the position the vehicles achieved max speed at 50 km/h as such the constant running condition. No idling time was achieved on the track section.

And we were only interested in the sound power level on position A.

The output file will only have the equivalent sound power level calculated. This is because noise exposure is calculated only using equivalent levels according to the CNOSSOS method. But the software will create an excel file containing other relevant levels, such as total rolling and traction sound power level. In the Vehicle and Track files, the parameters from appendix 6.1 - 6.8 is found, and its possible to add new trains, tracks or new parameters. Such as the rail roughness levels that has been measured.

3.5 Comparison between models and measurements

To examine if our model is accurate we compared the spectrum for the measured and modelled maximum sound levels. We made the approximation that the maximum sound level was the energetic sum of the noise contribution from two wheels when the microphone was positioned perpendicular to the centre of the boogie. To model the maximum sound level from the train, we used equation 2.21 and calculated the sound power from each axle on the vehicle. Then we used equation 2.22 to model how the sound propagated with attenuation from the geometric divergence and ground effects. The distance between the track and the microphone was measured on site in table 3.6, and the spacing between the wheels were assumed to be 1m.

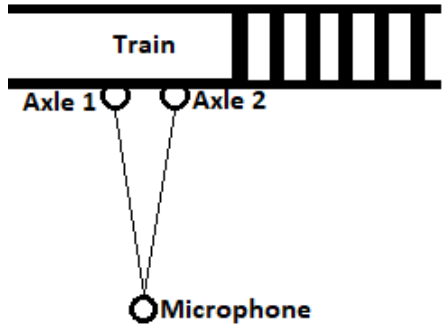

Figure 3.16: Assumed position of train as maximum sound level is modelled

To determine the accuracy of the model we will look the average error level L_{avg} for each modelled spectrum. The average error level is calculated from the difference between the measured and modelled maximum sound level at each 1/3 octave band n.

$$L_{avg} = \sum_{n} \frac{|L_{n,measured} - L_{n,modelled}|}{n} \tag{3.1}$$

3.6 Data acquired from Brekke & Strand

In this section we will present the data from measurements by consultants at Brekke&Strand. The data presented are the rail roughness levels and maximum sound pressure levels for each geographical position. The date the measurements were conducted is presented in table 3.10.

Table 3.10: Dates for measurements

Type of Measurement	Tjernsrud	Dalbakkveien	Linderudveien	Åsjordet
Maximum sound level	31/05-16	01/07-16	04/05-16	02/06-16
Rail rougness level	16/6-16 and 17/6-16			

3.6.1 Rail roughness levels

These results are the measured arithmetic average roughness levels from the centre line of the rail for the outgoing and ingoing track at each geographical position. Compared to the recommended upper limit from the standard EN ISO 3095:2013. Only the results from the centre line of the rail is used in this thesis because it is assumed to have the largest impact on the sound power level generated. As the RSA analyzer is limited to a range from 0.3 to 500mm in wavelength the upper and lower values outside this range are interpolated values.

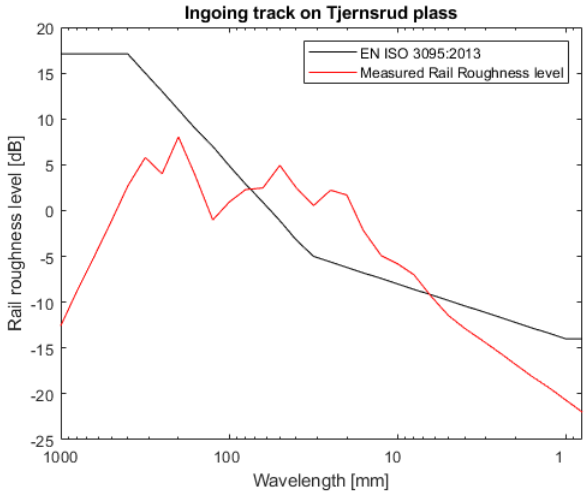

Figure 3.17: Measured rail roughness level on ingoing track and upper limit from ISO 3095 at Tjernsrud plass.

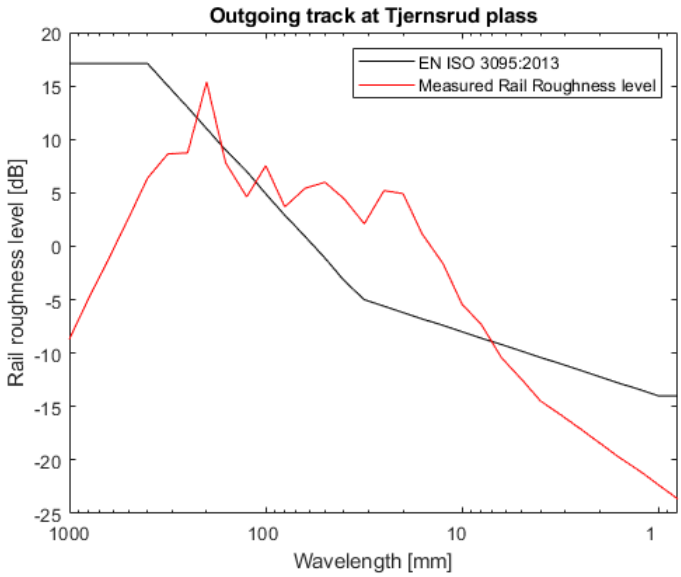

Figure 3.18: Measured rail roughness level on outgoing track and upper limit from ISO 3095 at Tjernsrud plass.

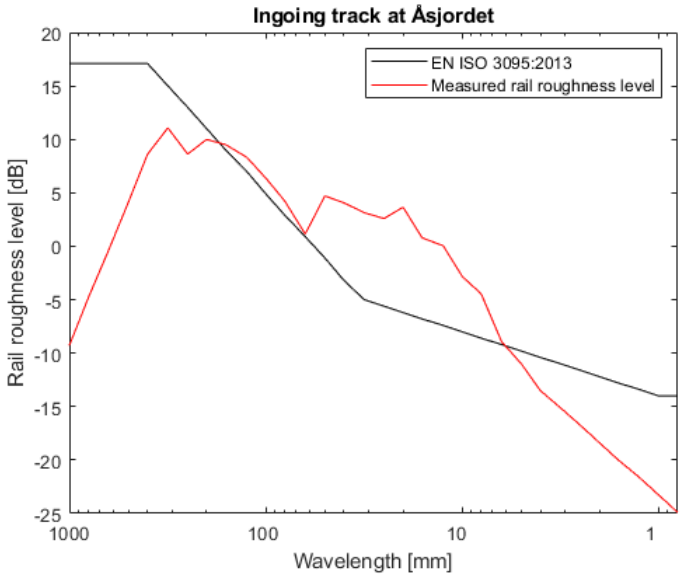

Figure 3.19: Measured rail roughness level on ingoing track and upper limit from ISO 3095 at Åsjordet.

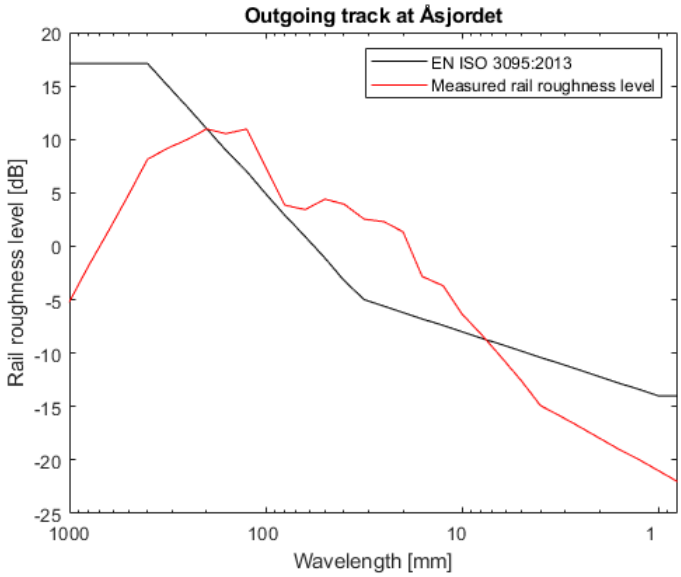

Figure 3.20: Measured rail roughness level on outgoing track and upper limit from ISO 3095 at Åsjordet.

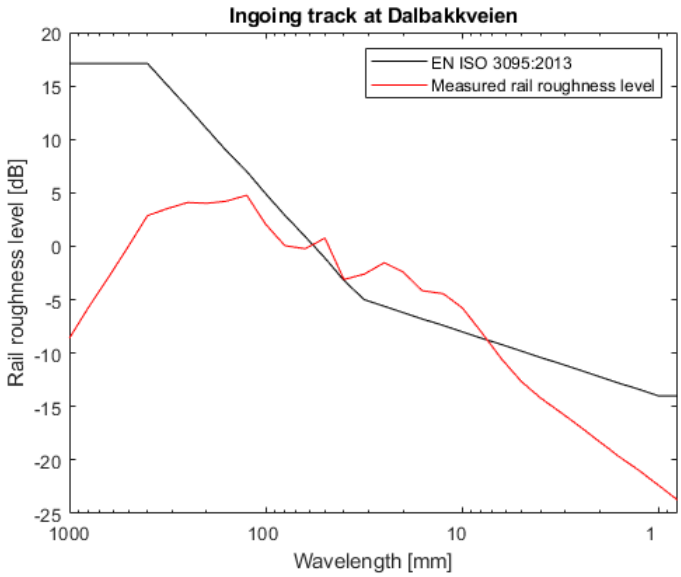

Figure 3.21: Measured rail roughness level on ingoing track and upper limit from ISO 3095 at Dalbakkveien.

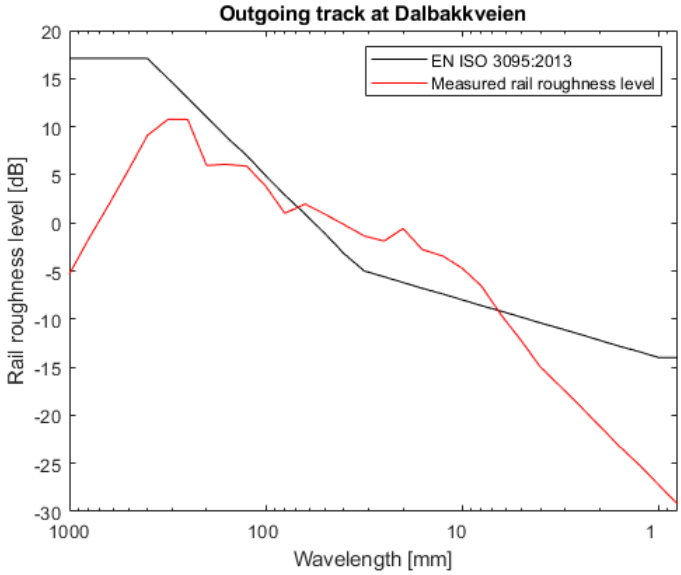

Figure 3.22: Measured rail roughness level on outgoing track and upper limit from ISO 3095 at Dalbakkveien.

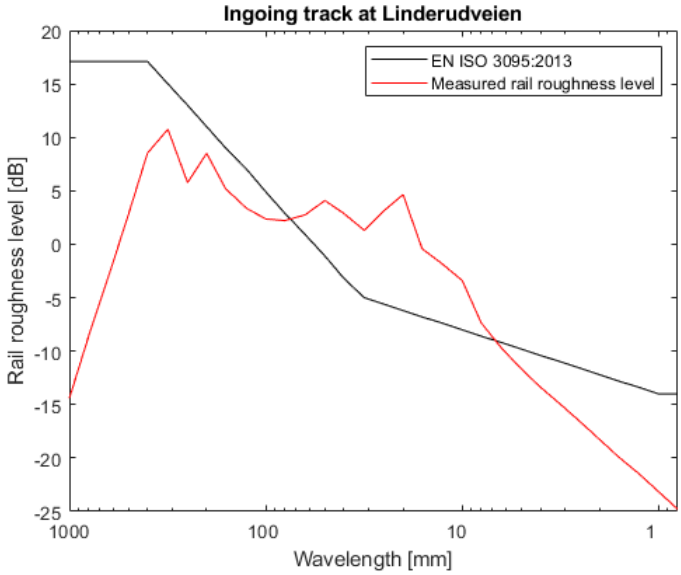

Figure 3.23: Measured rail roughness level on ingoing track and upper limit from ISO 3095 at Linderudveien.

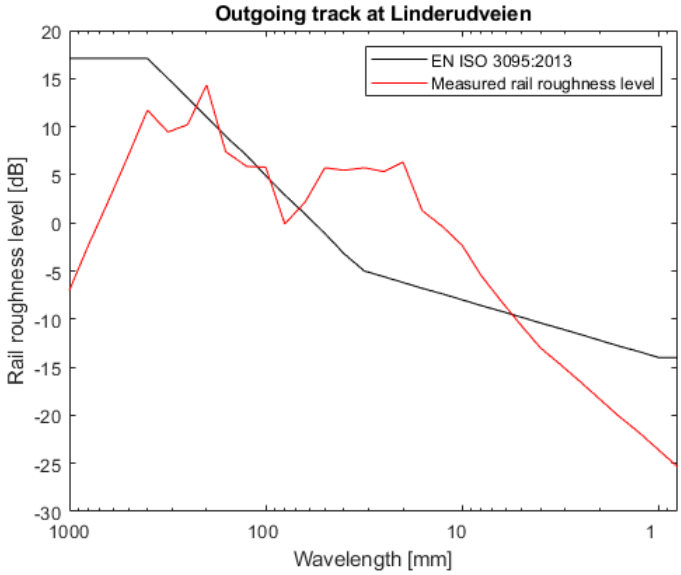

Figure 3.24: Measured rail roughness level on outgoing track and upper limit from ISO 3095 at Linderudveien.

3.6.2 Maximum sound levels acquired by Brekke & Strand

In this section we present the measured maximum sound levels in 1/3 octave bands for each individual measured tram and metro. The maximum sound level of each unique tram and metro that pass by is represented with a dotted line. We have also plotted the logarithmic average at each geographical position. The maximum sound levels are unweighted in the frequency spectrum and with a fast time weighting.

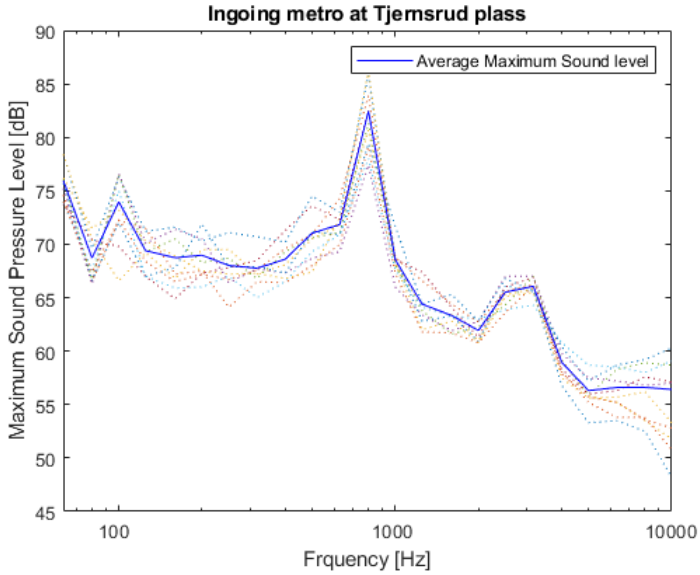

Figure 3.25: Maximum sound level from multiple passby measurements on ingoing metro at Tjernsrud plass.

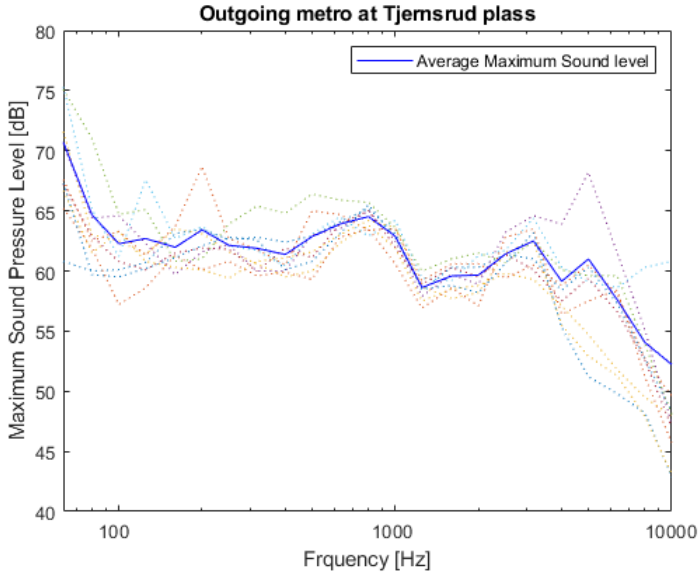

Figure 3.26: Maximum sound level from multiple pass by measurements on outgoing metro at Tjernsrud plass.

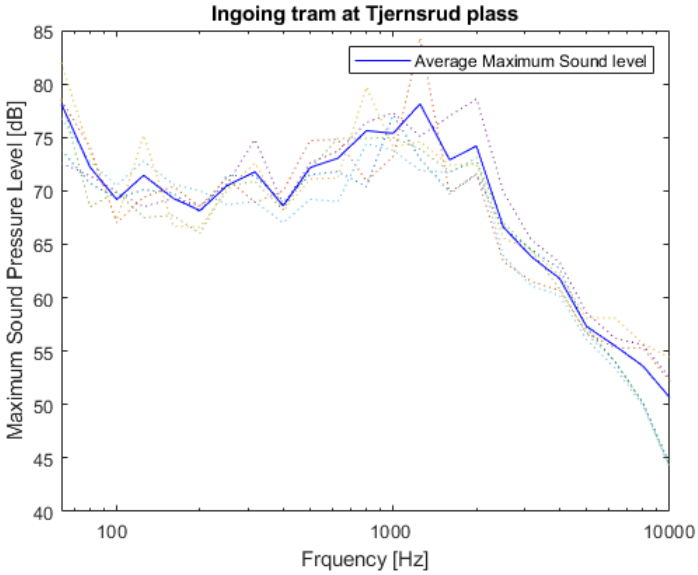

Figure 3.27: Maximum sound level from multiple passby measurements on ingoing tram at Tjernsrud plass.

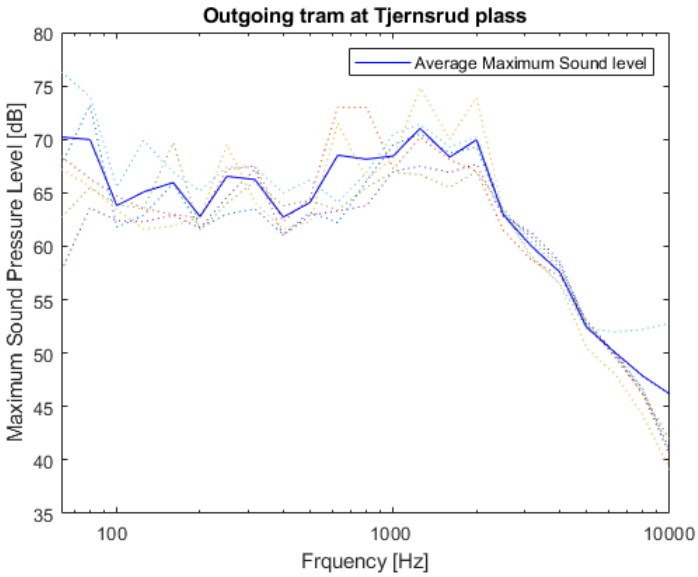

Figure 3.28: Maximum sound level from multiple passby measurements on outgoing tram at Tjernsrud plass.

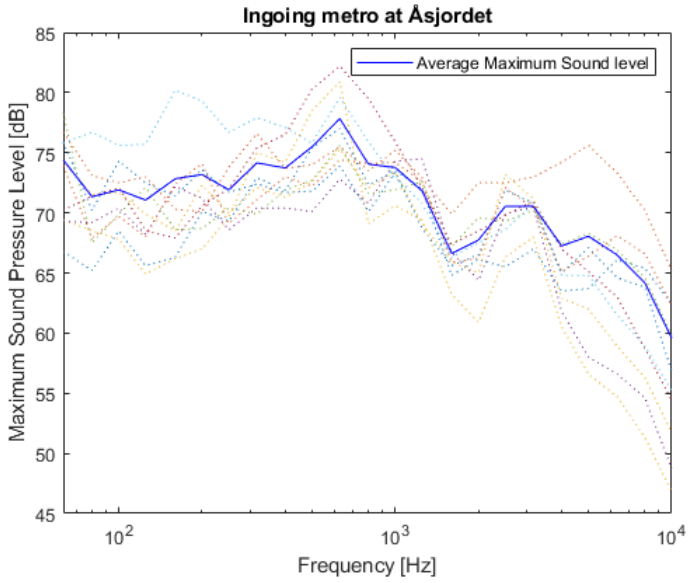

Figure 3.29: Maximum sound level from multiple pass by measurements on ingoing metro at Åsjordet.

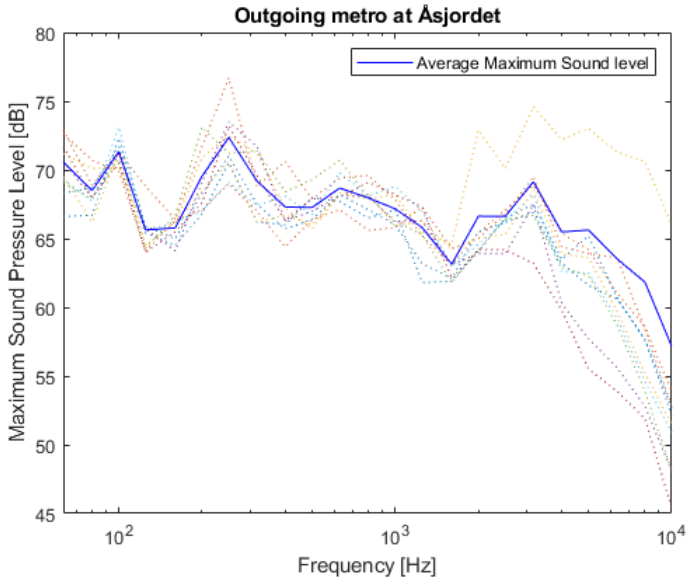

Figure 3.30: Maximum sound level from multiple pass by measurements on outgoing metro at Åsjordet.

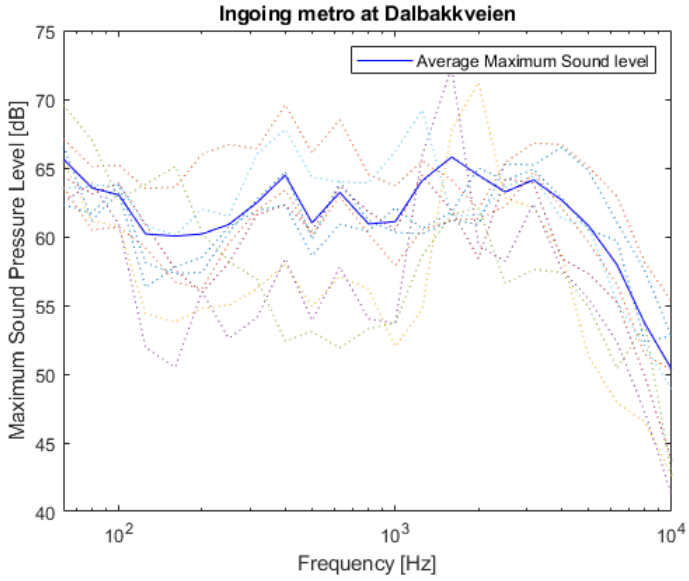

Figure 3.31: Maximum sound pressure level from multiple pass by measurements on ingoing metro at Dalbakkveien.

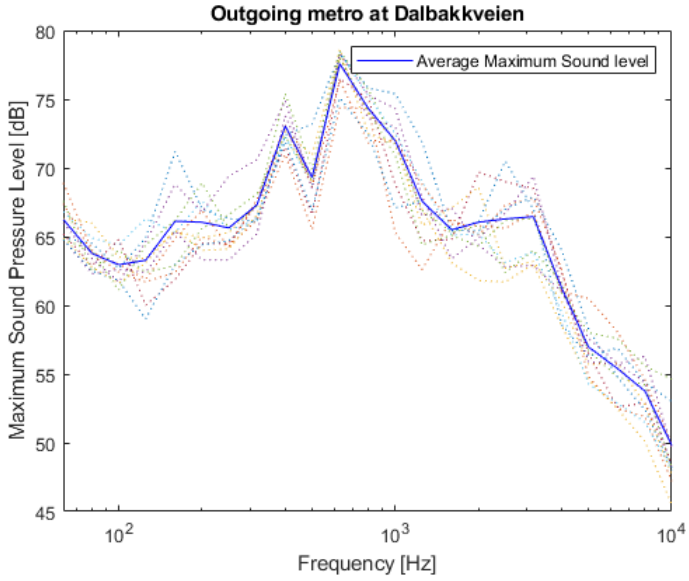

Figure 3.32: Maximum sound pressure level from multiple pass by measurements on outgoing metro at Dalbakkveien.

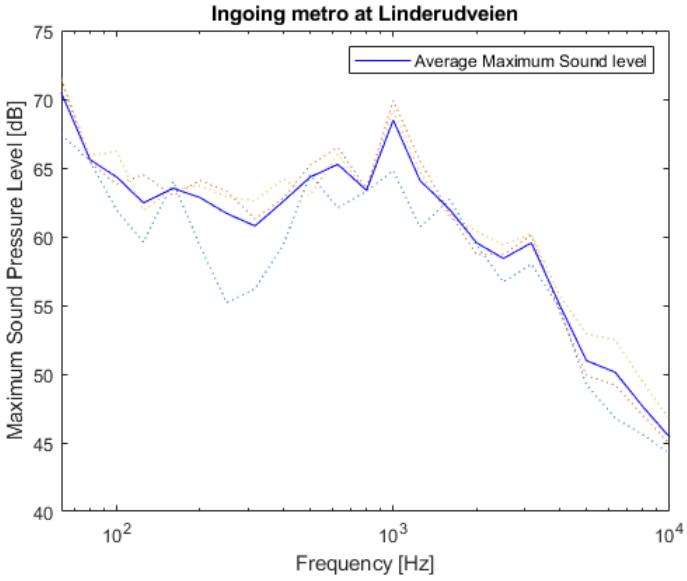

Figure 3.33: Maximum sound pressure level from multiple pass by measurements on ingoing metro at Linderudveien.

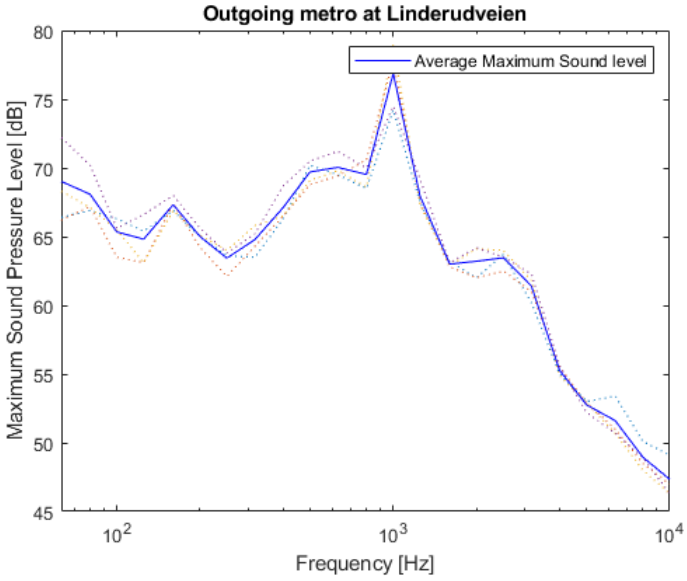

Figure 3.34: Maximum sound pressure level from multiple pass by measurements on outgoing metro at Linderudveien.

Chapter 4

Results

The first part of this chapter present the results from the measurements with the acoustical camera. The second part will look at a comparison between the measured and modelled maximum sound level. Finally, we will look at the average error level of the spectrum for each modelled case. We will present the results from each individual geographical position, because they are not comparable, due to different rail roughness levels and positioning of microphones.

4.1 Acoustic Camera

In this section we will look at the data captured with the acoustical camera. The result is presented in two sections, one for the SL-95 tram and one for the MX3000 metro. The results are given for one pass by with the camera positioned at approximately position A (0.5m) and B (4m). The measurements were conducted on the 14th February for height A, and 30th January for height B. Multiple passes were measured, but only one typical pass at each height of the train is presented in this section. As no new information were obtained from multiple measurements with the camera. The tram and metro is outgoing when measured at height A and ingoing at height B.

4.1.1 SL-95

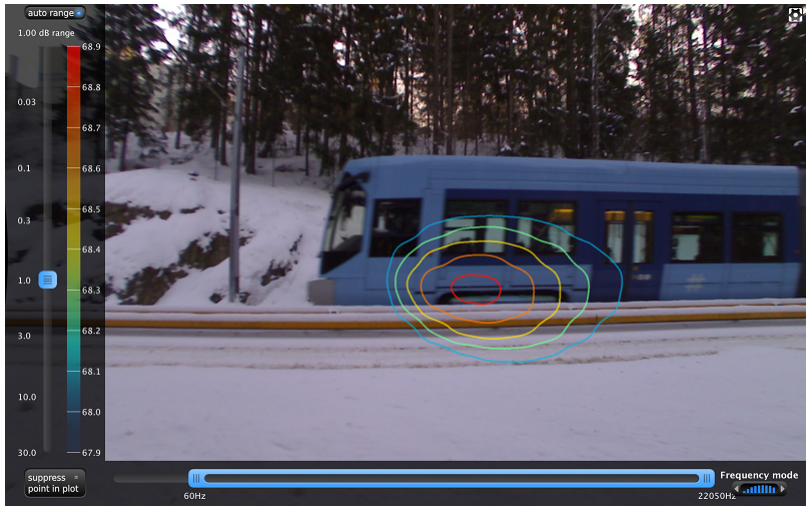

Figure 4.1: Acoustic camera measurement of first vehicle on SL-95 tram at height A.

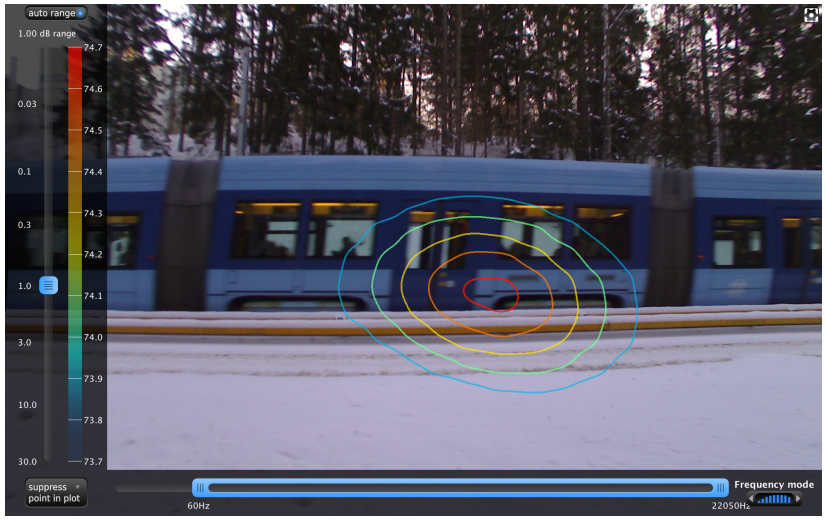

Figure 4.2: Acoustic camera measurement of second vehicle on SL-95 tram at height A.

Figure 4.3: Acoustic camera measurement of third vehicle on SL-95 tram at height A.

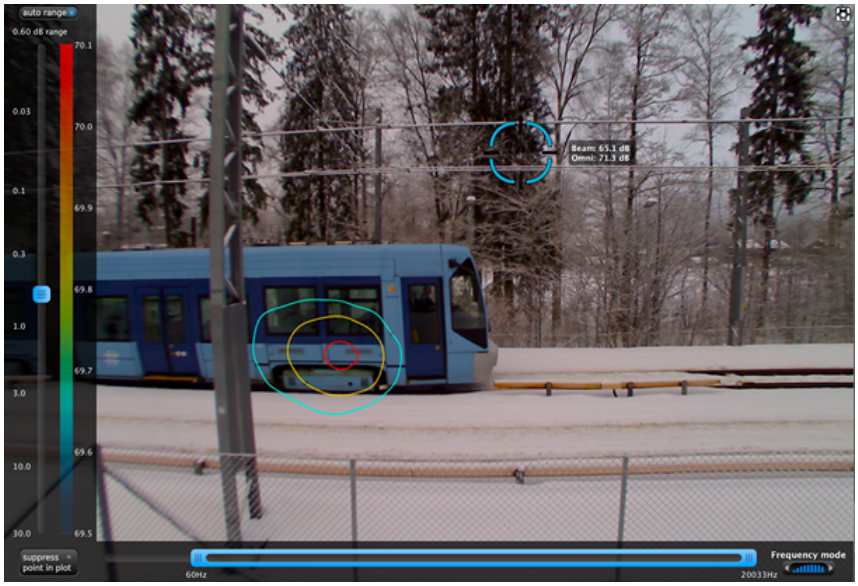

Figure 4.4: Acoustic camera measurement of first vehicle on SL-95 tram at height B.

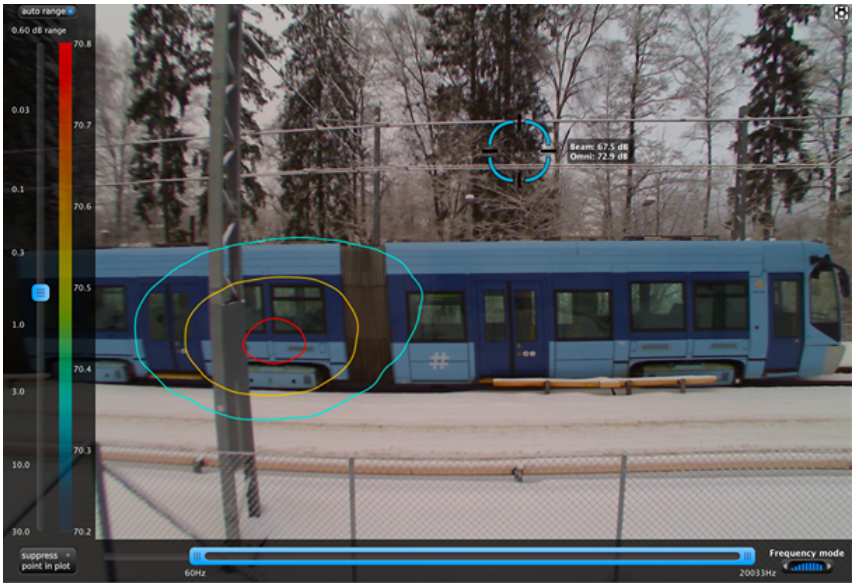

Figure 4.5: Acoustic camera measurement of second vehicle on SL-95 tram at height B.

Figure 4.6: Acoustic camera measurement of third vehicle on SL-95 tram at height B.

Figure 4.7: Acoustic camera measurement of first vehicle on SL-95 tram at height B with frequency spectrum from 2kHz to 20kHz

4.1.2 MX3000

Figure 4.8: Acoustic camera measurement of first vehicle on MX3000 train.

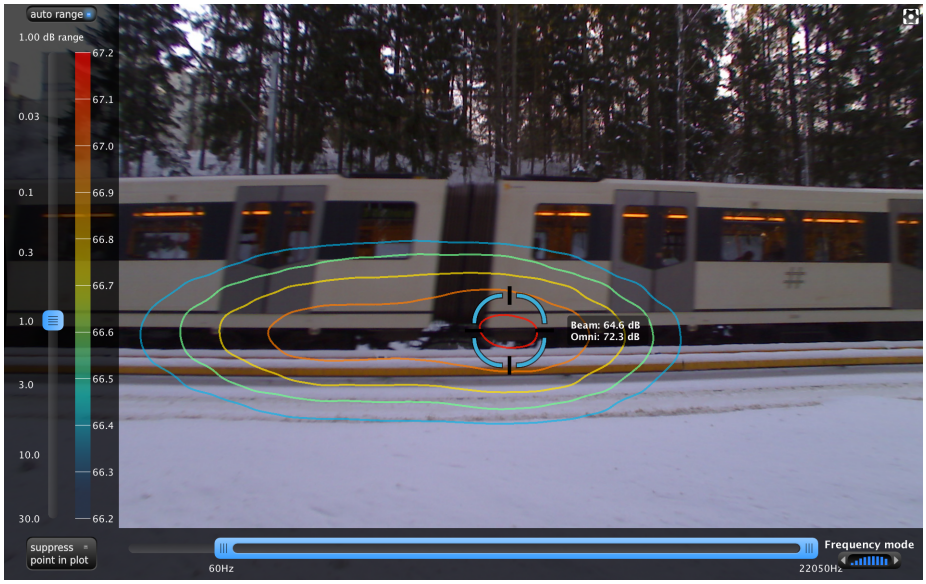

Figure 4.9: Acoustic camera measurement of first and second vehicle on MX3000 train.

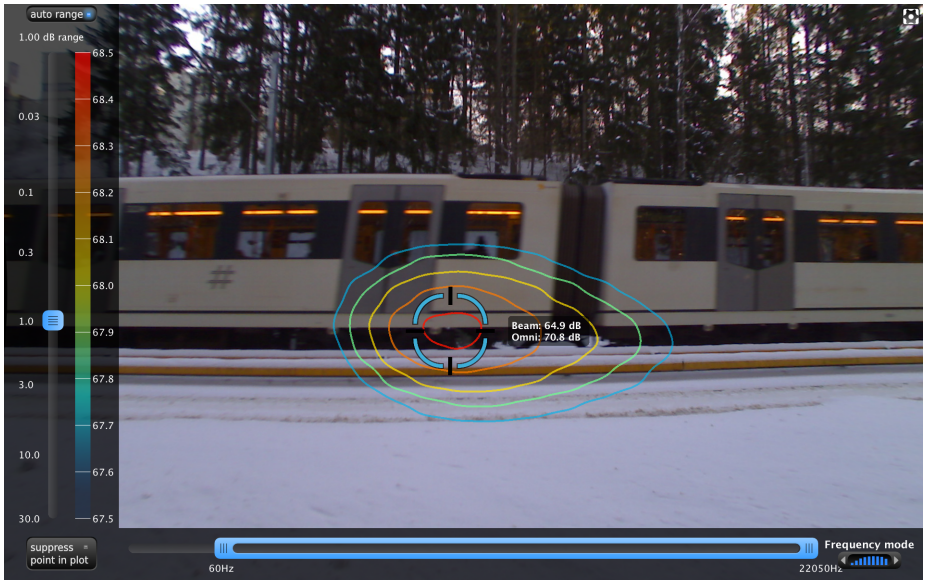

Figure 4.10: Acoustic camera measurement of second and third vehicle on MX3000 train.

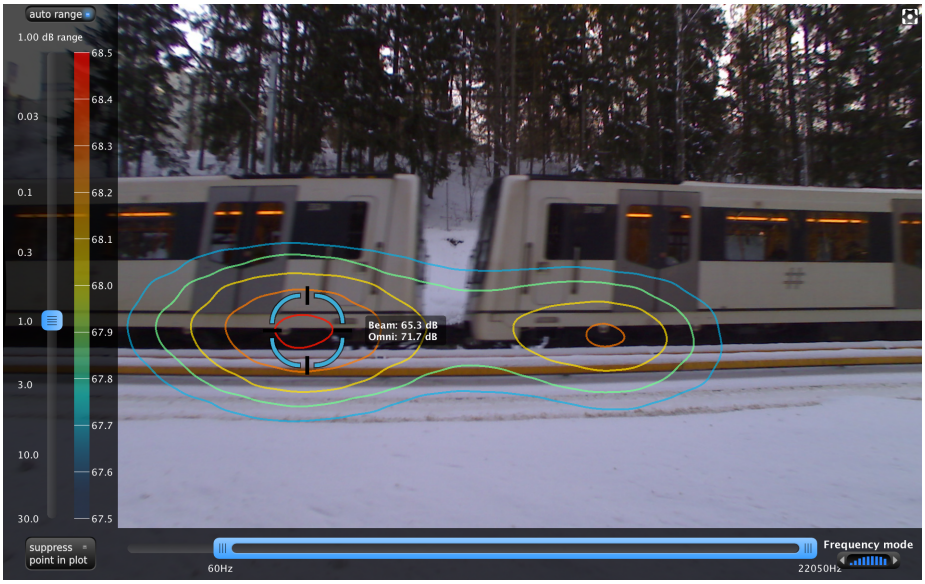

Figure 4.11: Acoustic camera measurement of third and fourth vehicle on MX3000 train.

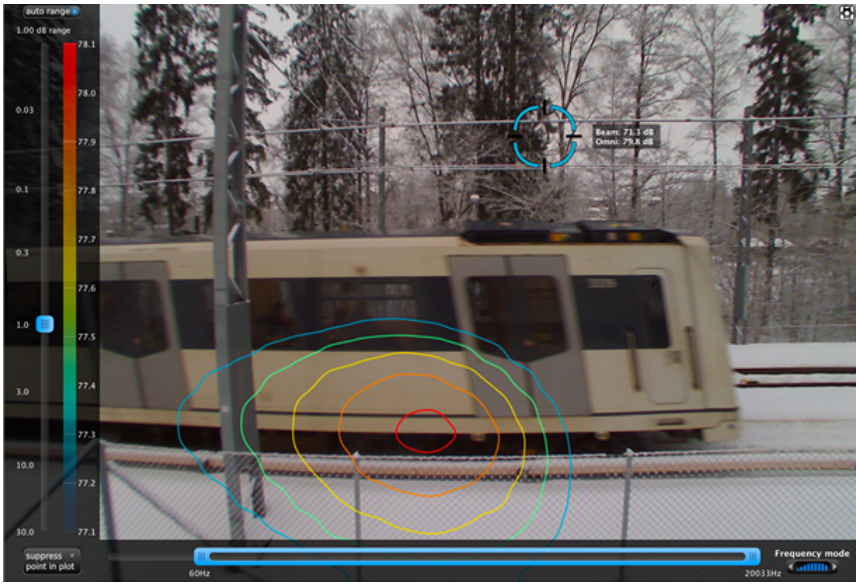

Figure 4.12: Acoustic camera measurement of first vehicle on MX3000 train at height B.

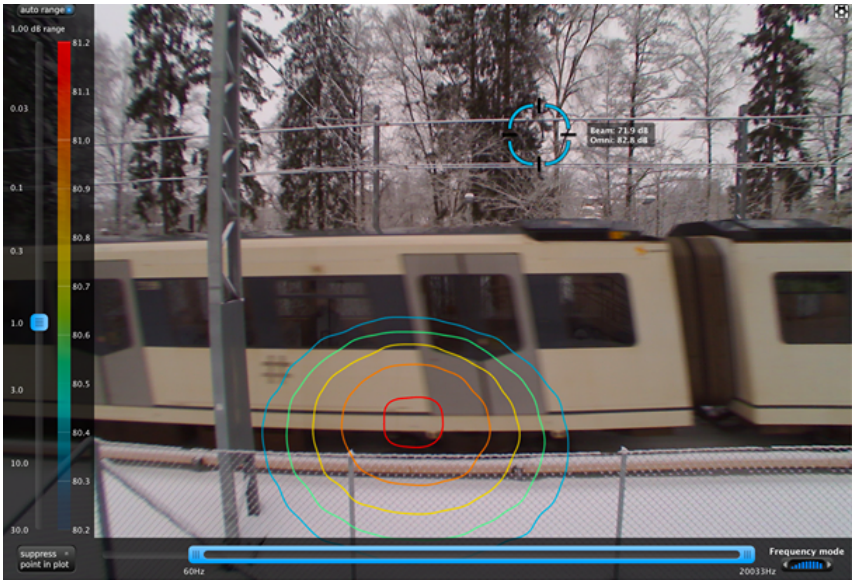

Figure 4.13: Acoustic camera measurement of first and second vehicle on MX3000 train at height B.

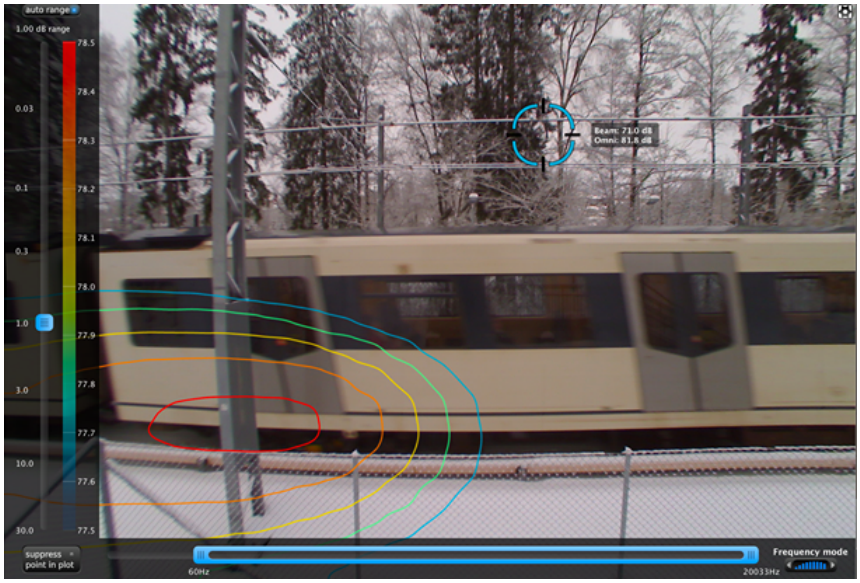

Figure 4.14: Acoustic camera measurement of second vehicle on MX3000 train at height B.

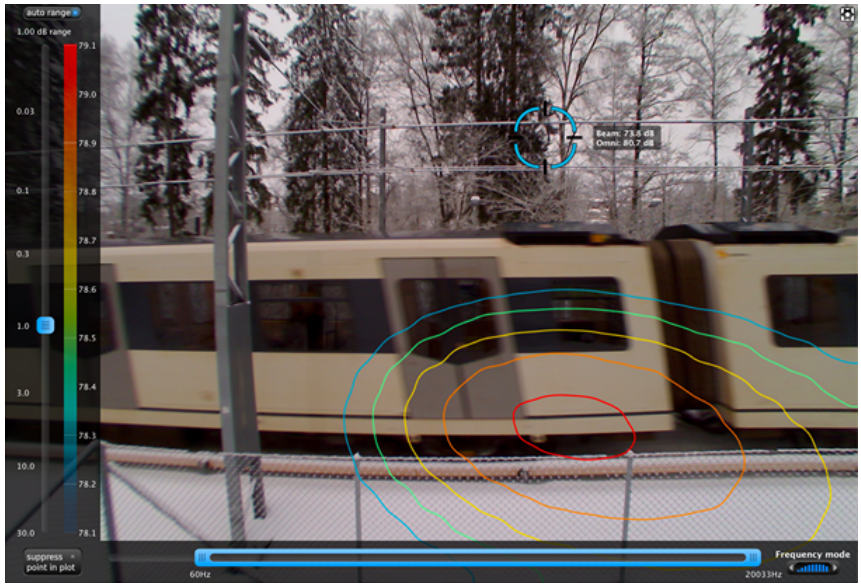

Figure 4.15: Acoustic camera measurement of second and third vehicle on MX3000 train at height B.

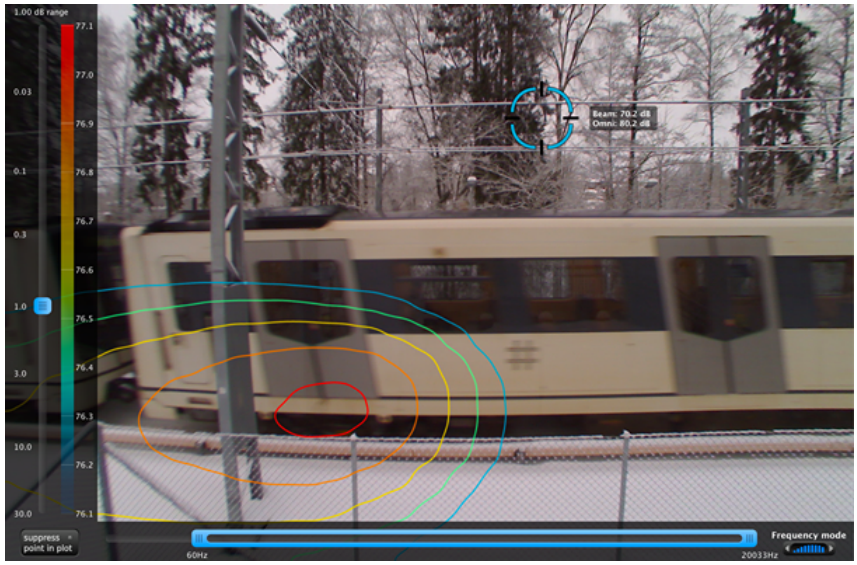

Figure 4.16: Acoustic camera measurement of third vehicle on MX3000 train at height B.

4.2 Comparison of measured and modelled maximum sound level

In this section we will look at the comparison of spectra for the modelled maximum sound level and measured maximum sound level at each geographical position, according to the CNOSSOS method described in section 3.5. The modelled maximum sound level is based on two different cases. One where the rail roughness is measured on site, and one where the rail roughness is assumed to be according to the upper limit in ISO 3095. The measured maximum sound level is still unweighted and with a fast dispersion. The modelled maximum sound level is achieved using the method described in section 3.5. The plots are not comparable to each other as each location has its own individual parameters.

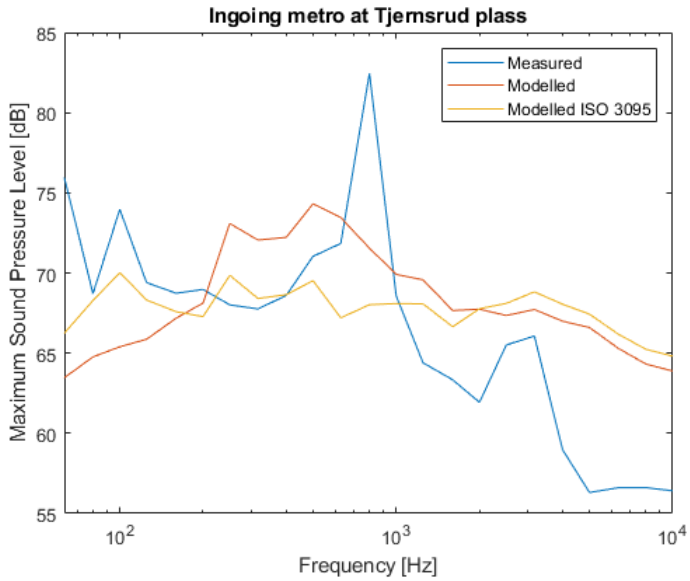

Figure 4.17: Comparison of the modelled and arithmetic average maximum sound level on ingoing metro Tjernsrud plass.

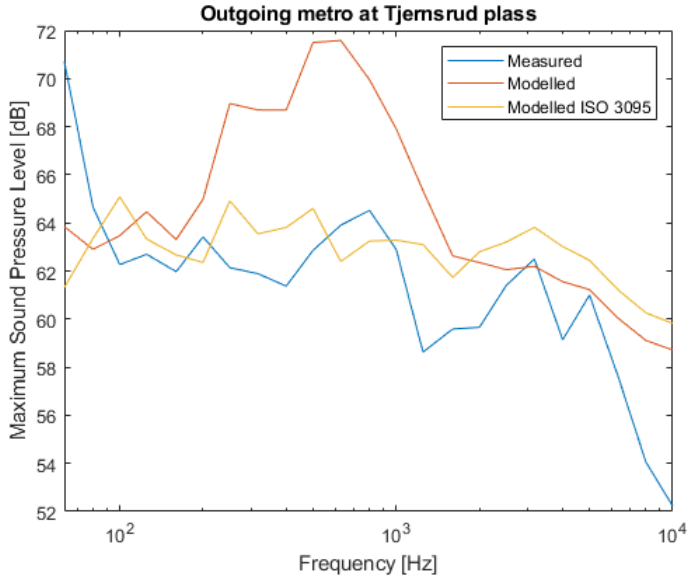

Figure 4.18: Comparison of the modelled and arithmetic average maximum sound level on outgoing metro at Tjernsrud plass.

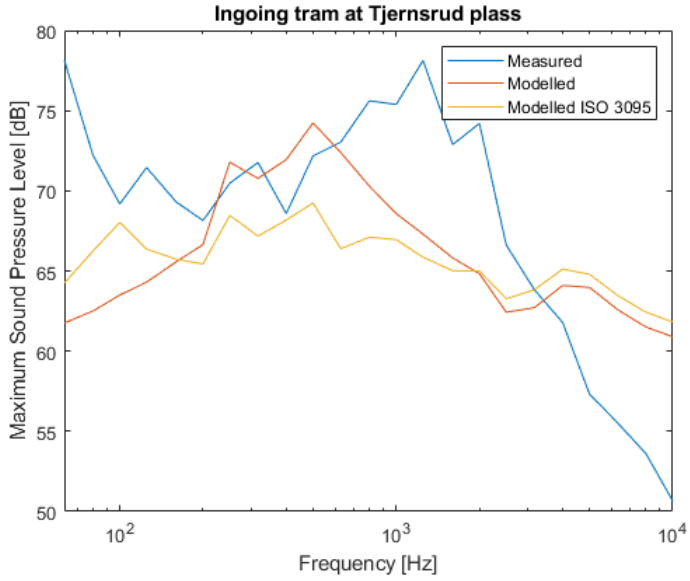

Figure 4.19: Comparison of the modelled and arithmetic average maximum sound level on ingoing tram at Tjernsrud plass.

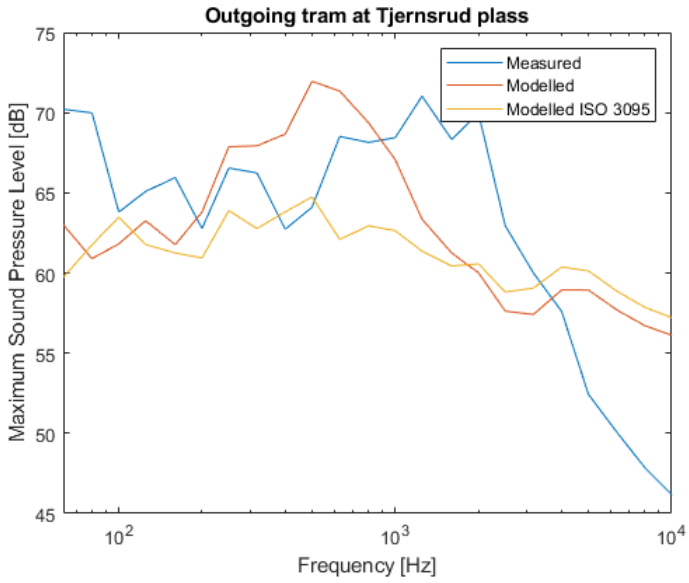

Figure 4.20: Comparison of the modelled and arithmetic average maximum sound level on outgoing tram at Tjernsrud plass.

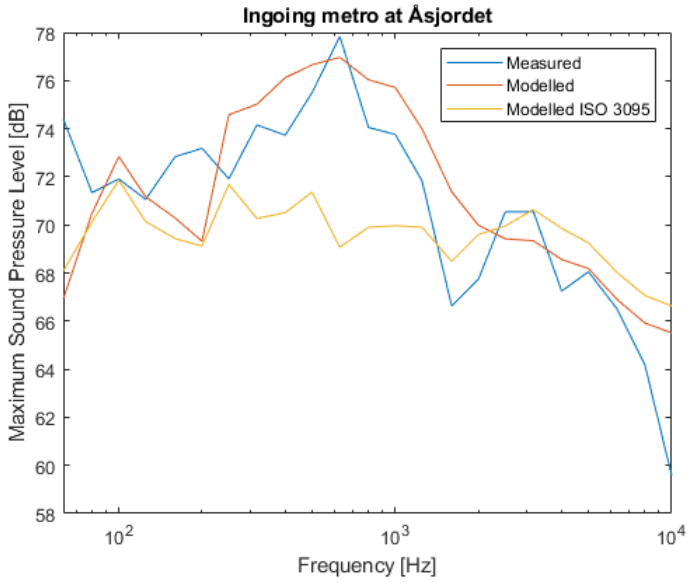

Figure 4.21: Comparison of the modelled and arithmetic average maximum sound level on ingoing metro at Åsjordet.

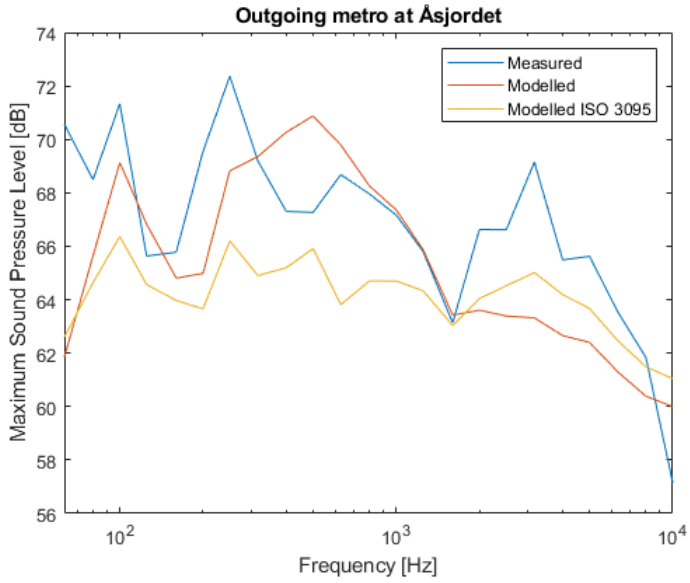

Figure 4.22: Comparison of the modelled and arithmetic average maximum sound level on outgoing metro at Åsjordet.

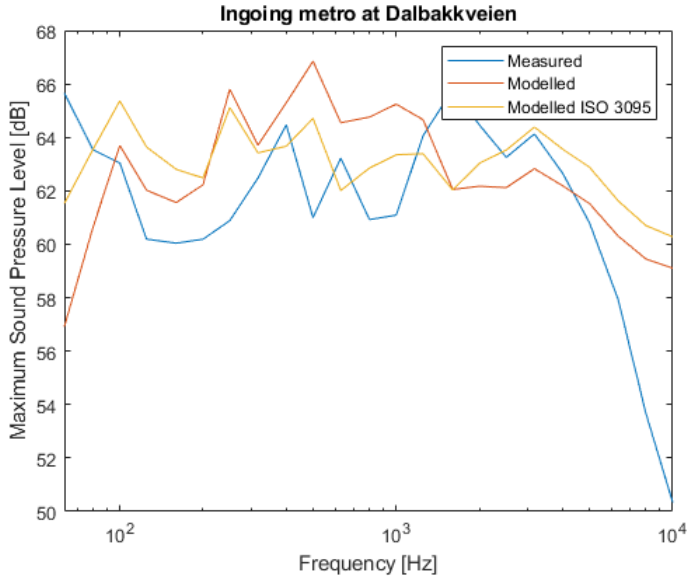

Figure 4.23: Comparison of the modelled and arithmetic average maximum sound level on ingoing metro at Dalbakkveien.

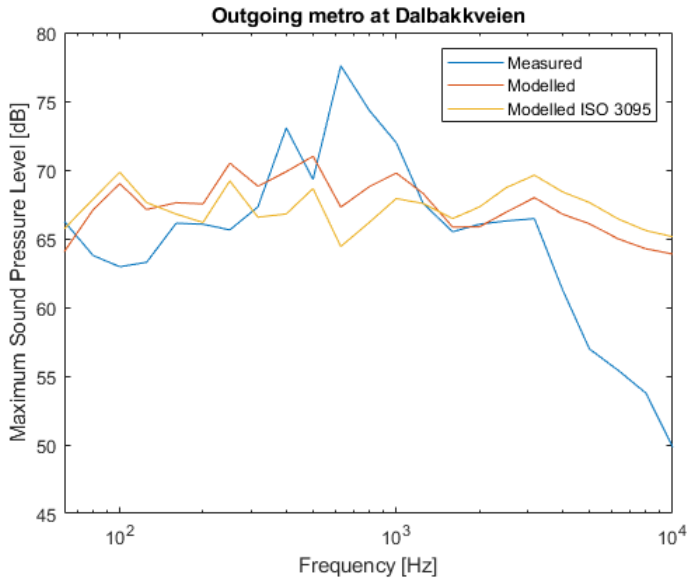

Figure 4.24: Comparison of the modelled and arithmetic average maximum sound level on outgoing metro at Dalbakkveien.

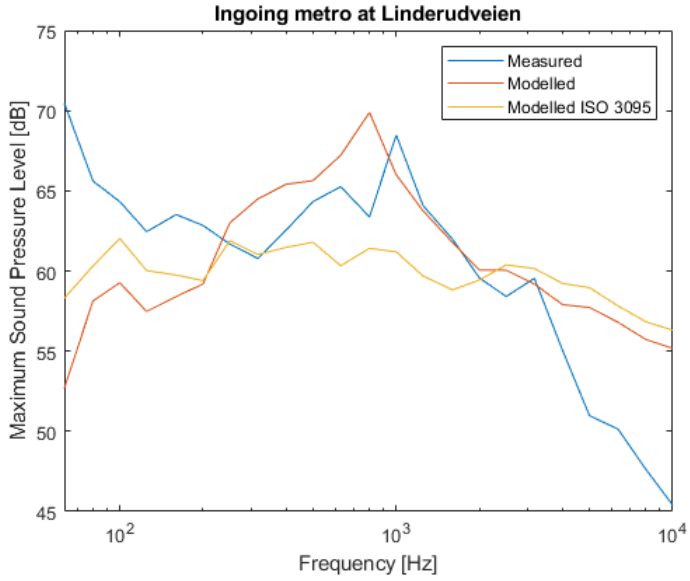

Figure 4.25: Comparison of the modelled and arithmetic average maximum sound level on ingoing metro at Linderudveien.

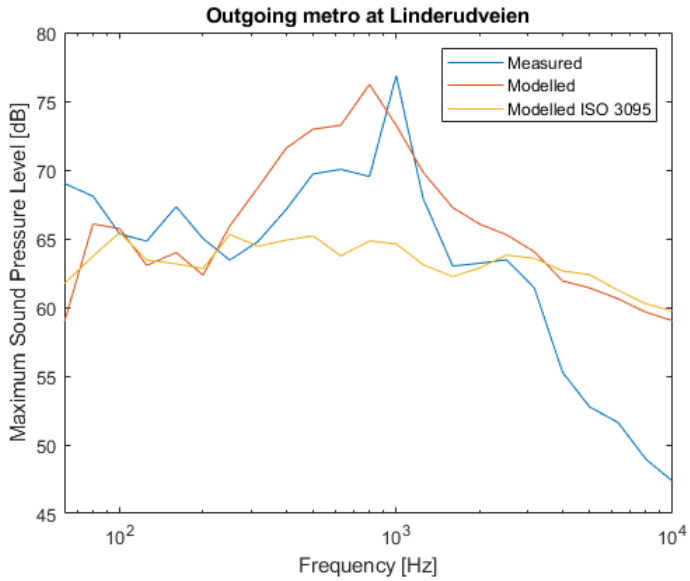

Figure 4.26: Comparison of the modelled and arithmetic average maximum sound level on outgoing metro at Linderudveien.

4.2.1 Average error level between models and measurement

In addition to the comparison in the previous section, we have calculated the average error level in the spectrum for our models compared to the spectrum of the measured maximum sound level. This is done for the 1/3 octave band from 63Hz to 10kHz at each location and it is presented in table 4.1 and 4.2. The average error level is calculated according to section 3.5.

Table 4.1: Average error level [dB] for the metro model

	Tjernsrud		Åsjordet		Dalbakkveien		Linderudveien	
Direction of travel	In	Out	In	Out	In	Out	In	Out
Average error level with measured rail roughness	5.3	4.0	2.1	2.5	2.9	4.3	4.4	4.7
Average error level with rail roughness from ISO 3095	4.6	2.8	2.9	3.0	2.6	5.1	4.3	4.8

Table 4.2: Average error level [dB] for the tram model

	Tjernsrud plass	
Direction of travel	In	Out
Average error level with measured rail roughness	5.7	5.0
Average error level with rail roughness from ISO 3095	6.0	5.5

Chapter 5

Analysis

5.1 Measurements with Acoustic Camera

In section 4.1 we can see the sources that emit noise at the frequency range 63Hz to 20kHz on the train and metro. Section 4.1.1 looks at the SL-95 tram and section 4.1.1 the metro train MX3000. Figure 4.1,4.3 and 4.4 pinpoints the boogie closest in the image as the dominant source. In figure 4.2 images from the camera shows that the front of boogie number 3 is the loudest one. In figure 4.5 and 4.6 we can see that the strongest source is second boogie set on the tram. On further inspection it seems like the slit between the boogie screen and the superstructure is the location where the rolling noise emerges from. This corresponds well with our height A at 0.5m. The camera also presents the sound coming from each boogie as one point source. This could be due to the fact that it struggles to separate the noise from each of the wheels as it is of low frequency and the camera is positioned to far away from the track. The camera can not identify dominant sources at height B when using the frequency spectrum that we chose from 63Hz to 20kHz. If we change the frequency spectrum to span from 2kHz to 20kHz we can identify a sound source under the pantograph in figure 4.7. But the sound level from this part of the spectrum and source is 30dB weaker than from the overall sound level that the train emit in figure 4.4. And we can not identify the pantograph as a noise source when looking at the total maximum sound level. This could be due to rolling noise dominating the whole spectrum and masking this particular source. We do know that equipment that makes noise is positioned at the roof, but apparently under these conditions they are not operating such that their noise level is noticeable. The acoustical camera were also used in cold temperatures which means that there might be less requirement for cooling equipment such as fans to be operating.

Section 4.1.2 looks at the noise pattern emitted from the MX3000 metro. In figure 4.7, 4.9, 4.11, 4.12, 4.13, 4.14 and 4.15 it is the boogie closest to the camera that emits dominating noise. In figure 4.8, the camera indicate that the second and third boogie are almost equal in emitted sound level. It does the same in figure 4.10, but now it is the last boogie of the first vehicle, and the first boogie of the last vehicle that is identified as one source.

MX3000 does not have a screen in front of the wheels, and the noise seems to be emerging at the edge of the superstructure. Similar to the tram, each boogie is identified as one point source. No source at height B seems to be emitting any noise for our frequency spectrum. The drive train and engine is positioned behind the wheel, and any engine noise will probably be masked by the rolling noise from the wheels.

5.2 Previously collected data with Rail roughness and Maximum sound level

None of the rail roughness levels in section 3.6.1 are lower than the recommended upper limit from EN ISO 3095:2013. The wavelengths from 100mm to 10mm are exceeding the limit for each measurement. These wavelengths would correspond to approximately from 125Hz to 1250Hz. The interpolated roughness levels from 500mm and upwards are decreasing quickly. The same applies for the wavelengths below 3.15mm. Each rail roughness measurement is relative similar to each other in their distribution throughout their spectrum. This could be due to the fact that rolling stock are identical on each part of the track. As such it would wear on the tracks in a similar pattern, except on Tjernsrud Plass, where both the metro and tram is operated. The rail grinding schedule could also impact the roughness level.

The measured maximum sound level in section 3.6.2 is unfortunately based on few measurements, but this was the only data we had access to. In figure 3.25 a strong peak at 800Hz is present. The outgoing metro in figure 3.26 does not have this peak . Further, the figure 3.27 and 3.28 show the tram pass by measurements. As mentioned, the only data we have of the tram is on Tjernsrud plass. The ingoing metro at Åsjordet, in figure 3.29, has higher variance for each passby, compared to the outgoing metro in figure 3.30. The same can be accounts for the measurements from Dalbakkveien. Linderudveien is the case with the fewest measurements. We can see that each passing train can vary in maximum sound level at each geographical position, indicating that each train set has its own unique noise spectrum. This is best visualised in figure 3.31 where the train with the lowest sound level at 630Hz is almost 15 dB less loud than the loudest train at this frequency. At last we can see that all the spectra have strongly decreasing maximum sound levels after 3160 Hz.

5.3 Comparison of measurement and model

In figure 4.16 we can immediately see a large peak at 800Hz previously mentioned, this could be due to curve squeal as it occurs for all trains and it has a tonal feature, but curve squeal is not noted in the logbook and we do not have the recording of the data to investigate it any further. Both models are struggling to produce the same result. And both models are overestimating the maximum sound level above 3160Hz. For the outgoing metro in figure 4.17 we have a large modelled peak between 250 Hz and 1kHz compared to the measured data. The ISO 3095 model is more similar to the measured results. The comparison in figure 4.18 shows a large variation between the model and measurement over the whole spectrum for the model with measured rail roughness. The rail roughness

from IS0 3095 is more accurate. This is equal to the the modelled sound level in figure 4.19. Figure 4.20 and 4.21 displays the model and measurements that are the most accurate of all the cases. Here the ISO 3095 model underestimates the maximum sound level. The models in figure 4.22 are mostly accurate below 3160Hz, but they are less accurate at the higher frequencies. The outgoing metro in figure 4.23 has a predominant peak at 630Hz. The models are inaccurate above 3160Hz where they are modelling the maximum sound level to high. At Linderudveien the model with measured rail roughness, calculates the peak at 800Hz very accurately. While the model with ISO 3095 rail roughness fails to imitate this dominant peak. Both models struggle however with simulating the loss after 3160Hz.

It seems like all the models are overestimating the sound power emitted in the higher frequencies above 3kHz. In the middle and lower frequency range, the models seems to be more accurate. According to table 4.1, the best modelling scenario for the metro is calculated on the Åsjordet section. And the worst overall modelling is at Tjernsrud plass. Looking further at table 4.1 and 4.2 we see no clear tendency toward that using the on site rail roughness level is any better than using the upper limit rail roughness level from ISO 3095. This could be because those two levels are overall quite similar. However, if we look at the spectra of each case, we can see that the models with measured rolling roughness can imitate sudden peaks like the one in figure 4.25. There is no evidence supporting the theory that the position of the microphone will improve the results in our method.

We would like to mention potential sources of error to our models. The sound power level is calculated from tables in the Annex We could choose other contact filers and transfer function coefficients from the CNOSSOS supported tables which could maybe give better modelling results, but then the assumed physical properties would deviate more from the real rolling stock. And we would be loosing the purpose of describing accurately the train according to the CNOSSOS method.

The sound propagation model in this thesis does not take into account the reflections from buildings. We did not manage to implement it. And we believe that it could affect the model as there are buildings in close proximity to where the measurements were conducted. In addition our propagation model assumes that only two axles on a train are emitting sound, when all the wheels on the train could potentially be contributing to the total maximum sound level modelled. A total of 80 pass by measurements were sampled, and more samples would be desirable to get a more accurate average level. As we can see in figure 3.31 the maximum sound level from a metro can vary substantially. The freshness of the rail roughness data could be questioned, and it would be desirable to have both maximum sound and rail roughness level measured on the same date. Another limitation is how close to the railway we can do the measurements, due to fences along the track. The assumption that the track does not make any curve squeal, might be incorrect. On-site confirmation would be desirable, or a properly straight rail section could be chosen.

Chapter 6

Conclusion

This thesis aimed at determining a noise emission model for the tram and metro in Oslo according to the method described in CNOSSOS. Physical properties on the trains and railway were examined to identify descriptors accordingly. An acoustical camera was used to study the equivalent noise sources on the trains, to further substantiate our choices of train descriptors. Maximum sound levels were modelled according to CNOSSOS and compared with measurements previously performed by consultants at Brekke & Strand.

Four different geographical locations were used as comparison scenarios as the amount of measurement data was sparse from only one location. We did not examine how the speed affected the noise emissions as all the measurement scenarios were conducted where the trains moved at approximately 45 km/h, except three cases where they moved at 34, 57 and 61 km/h. We compared the measured rail roughness with a defined limit from ISO 3095 at each location, to look at the influence it would have on the accuracy of our models. The results did not show a clear indication that the measured rail roughness level would improve our modelling, as compared to using a default value from ISO 3095. The overall average error level was almost equal between the model with measured rail roughness levels and the model with assumed rail roughness level from ISO 3095. The model with measured rail roughness would in some cases model large peaks correctly, but in other cases it would miss significant peaks. Both models overestimated the maximum sound level above 3kHz in all cases, except one.

The highest accuracy for one model was achieved on the ingoing metro at Åsjordet, with 2.1 dB in average error level for the scenario with measured rail roughness. We do not know why this particular model achieved this accuracy. It could be that reflections from buildings increase the measured maximum sound level and that this could fit the model better. As we did not take reflections into account in our calculations. We would not consider the accuracy of our model good enough, as there is a stated requirement that the input data should have accuracy better than $\pm$ 2 dB. And none of our models fulfils this requirement.

The models in this report can be improved by following the ISO 3095:2013 for measurements. Conducting more measurements and modelling the sound propagation with commercial software would improve the accuracy. Alternatively another comparison method could be used for increased simplicity and accuracy. As CNOSSOS does not calculate the maximum sound level, it could be better to compare the measured and modelled equivalent sound level.

Bibliography

[1] World Health Organization. Burden of disease from enviromental noise, 2011.

[2] Regjeringen.no. Felles støymetodikk, 2018.

[3] Marco Paviotti, Simon J. Shilton, Rick Jones, and Nigel Jones. Conversion of existing railway source data to use cnossos-eu, 2015.

[4] European Commission. Develop and implement harmonised noise assessment methods process applied to establish cnossos-eu/national method equivalence for rail source data. https://circabc.europa.eu/sd/a/ebfc8895-79fd-44db-8782-c5b26f6b1e37/CNOSSOS-EU%20Rail%20Equivalence%20Note_Final.pdf, 2012.

[5] P. De Vos. *Noise Mapping in EU: Models and Procedures*, chapter Railway Noise. Springer, 2012.

[6] Mikael Ögren and Johanna Bengtsson Ryberg. Bullerberäkningar med cnossos-eu i sverige, 2015.

[7] Jarno Kokkonen, Olli Kontkanen, and Panu Maijala. Cnossos-eu noise model implementation in finland, 2016.

[8] Lawrence E. Kinsler, Austin R. Frey, Alan B. Coppens, and James V. Sanders. *Fundamentals of Acoustics*. John Wiley & Sons, 4 edition, 2000.

[9] Gerhard Müller and Michael Möser. *Handbook of Engineering Acoustics*. Springer, 2013.

[10] Tor Erik Vigran. *Building Acoustics*. Taylor & Francis, 2008.

[11] David Thompson. *Railway Noise and Vibration*. Elsevier, 2009.

[12] Sigmund Olafsen. *Indoor Noise from Urban Railbound Transport*. PhD thesis, Lund University, 2016.

[13] Stylianos Kephalopoulos, Marco Paviotti, and Fabienne Anfosso-Lédée. Common noise assessment methods in europe, 2015.

[14] Hans G. Jonasson and Svein Storheier. Nord 2000: New nordic prediction method for rail traffic noise. *SP Rapport 2001:11*, 2001.

[15] Jørgen Grythe. Acoustic camera and beampattern. Technical note, Norsonic AS, 2018.

[16] Jacob Benesty, Jingdong Chen, and Yiteng Huang. *Microphone Array Signal Processing*. Springer, 2008.

[17] Jørgen Grythe. Evaluating array resolution. Technical note, Norsonic AS, 2018.

[18] Bane Nor. Teknisk regelverk. Official wiki page, https://trv.jbv.no/wiki/Forside, 1 2018.

[19] Pandrol Track Systems, 63 Station Road, Addlestone, Surrey KT15 2AR. *Fastclip FC Product Information*, 1 edition, 2016.

[20] Siemens, Mobility Division Nonnendammallee 101 13629 Berlin, Germany. *Metro - Oslo MX Norway*, 2014.

[21] AnsaldoBreda, via Argine 425- 80147 Napoli- Italia-. *Oslo LRV, SL-95*.

[22] Oskar Sivertsen. Lydfelt i smale bygater med trikketrafikk. Master's thesis, NTNU, july 2016.

[23] Norsonic. Akustisk kamera nor848a, 2017.

Appendix

Classification and descriptors for railway vehicles

Digit	1	2	3	4
Descriptor	**Vehicle type**	**Number of axles per vehicle**	**Brake type**	**Wheel measure**
Explanation of the descriptor	A letter that describes the type	The actual number of axles	A letter that describes the brake type	A letter that describes the noise reduction measure type
Possible descriptors	**h** high speed vehicle (> 200 km/h)	**1**	**c** cast-iron block	**n** no measure
	m self-propelled passenger coaches	**2**	**k** composite or sinter metal block	**d** dampers
	p hauled passenger coaches	**3**	**n** non-tread braked, like disc, drum, magnetic	**s** screens
	c city tram or light metro self-propelled and non-self-propelled coach	**4**		**o** other
	d diesel loco	etc.		
	e electric loco			
	a any generic freight vehicle			
	o other (i.e. maintenance vehicles etc.)			

Figure 6.1: Rail vehicle description table from [13]

Digit	1	2	3	4	5	6
Descriptor	**Track base**	**Railhead Roughness**	**Rail pad type**	**Additional measures**	**Rail joints**	**Curvature**
Explanation of the descriptor	Type of track base	Indicator for roughness	Represents an indication of the 'acoustic' stiffness	A letter describing acoustic device	Presence of joints and spacing	Indicate the radius of curvature in m
Codes allowed	**B** Ballast	**E** Well maintained and very smooth	**S** Soft (150-250 MN/m)	**N** None	**N** None	**N** Straight track
	S Slab track	**M** Normally maintained	**M** Medium (250 to 800 MN/m)	**D** Rail damper	**S** Single joint or switch	**L** Low (1 000-500 m)
	L Ballasted bridge	**N** Not well maintained	**H** Stiff (800-1 000 MN/m)	**B** Low barrier	**D** Two joints or switches per 100 m	**M** Medium (Less than 500 m and more than 300 m)
	N Non-ballasted bridge	**B** Not maintained and bad condition		**A** Absorber plate on slab track	**M** More than two joints or switches per 100 m	**H** High (Less than 300 m)
	T Embedded track			**E** Embedded rail		
	O Other			**O** Other		

Figure 6.2: Track description table from [13]

Wavelength	$L_{r,Tr,i}$			
	Min	Max	EN ISO 3095:2013 (Well maintained and very smooth)	Average network (Normally maintained smooth)
1 000 mm	– 15,0	22,0	17,1	11,0
800 mm	– 15,0	22,0	17,1	11,0
630 mm	– 15,0	22,0	17,1	11,0
500 mm	– 15,0	22,0	17,1	11,0
400 mm	– 15,0	22,0	17,1	11,0
315 mm	– 15,0	22,0	15,0	10,0
250 mm	– 15,0	22,0	13,0	9,0
200 mm	– 15,0	22,0	11,0	8,0
160 mm	– 15,0	22,0	9,0	7,0
120 mm	– 15,0	22,0	7,0	6,0
100 mm	– 15,0	22,0	4,9	5,0
80 mm	– 15,0	22,0	2,9	4,0
63 mm	– 15,0	22,0	0,9	3,0
50 mm	– 15,0	22,0	– 1,1	2,0
40 mm	– 15,0	22,0	– 3,2	1,0
31,5 mm	– 15,0	22,0	– 5,0	0,0
25 mm	– 15,0	22,0	– 5,6	– 1,0
20 mm	– 15,0	22,0	– 6,2	– 2,0
16 mm	– 15,0	22,0	– 6,8	– 3,0
12 mm	– 15,0	22,0	– 7,4	– 4,0
10 mm	– 15,0	22,0	– 8,0	– 5,0
8 mm	– 15,0	22,0	– 8,6	– 6,0
6,3 mm	– 15,0	22,0	– 9,2	– 7,0
5 mm	– 15,0	22,0	– 9,8	– 8,0
4 mm	– 15,0	22,0	– 10,4	– 9,0
3,2 mm	– 15,0	22,0	– 11,0	– 10,0
2,5 mm	– 15,0	22,0	– 11,6	– 11,0
2 mm	– 15,0	22,0	– 12,2	– 12,0
1,6 mm	– 15,0	22,0	– 12,8	– 13,0
1,2 mm	– 15,0	22,0	– 13,4	– 14,0
1 mm	– 15,0	22,0	– 14,0	– 15,0
0,8 mm	– 15,0	22,0	– 14,0	– 15,0

Figure 6.3: Track roughness coefficients table from [13]

Wavelength	$L_{x,VEH,i}$				
	Min	Max	Cast iron tread brake	Composite brake	Disk brake
1 000 mm	– 15,0	25,0	2,2	– 4,0	– 5,9
800 mm	– 15,0	25,0	2,2	– 4,0	– 5,9
630 mm	– 15,0	25,0	2,2	– 4,0	– 5,9
500 mm	– 15,0	25,0	2,2	– 4,0	– 5,9
400 mm	– 15,0	25,0	2,2	– 4,0	– 5,9
315 mm	– 15,0	25,0	2,2	– 4,0	– 5,9
250 mm	– 15,0	25,0	2,2	– 4,0	2,3
200 mm	– 15,0	25,0	2,2	– 4,0	2,8
160 mm	– 15,0	25,0	2,4	– 4,0	2,6
120 mm	– 15,0	25,0	0,6	– 4,0	1,2
100 mm	– 15,0	25,0	2,6	– 4,0	2,1
80 mm	– 15,0	25,0	5,8	– 4,3	0,9
63 mm	– 15,0	25,0	8,8	– 4,6	– 0,3
50 mm	– 15,0	25,0	11,1	– 4,9	– 1,6
40 mm	– 15,0	25,0	11,0	– 5,2	– 2,9
31,5 mm	– 15,0	25,0	9,8	– 6,3	– 4,9
25 mm	– 15,0	25,0	7,5	– 6,8	– 7,0
20 mm	– 15,0	25,0	5,1	– 7,2	– 8,6
16 mm	– 15,0	25,0	3,0	– 7,3	– 9,3
12 mm	– 15,0	25,0	1,3	– 7,3	– 9,5
10 mm	– 15,0	25,0	0,2	– 7,1	– 10,1
8 mm	– 15,0	25,0	– 0,7	– 6,9	– 10,3
6,3 mm	– 15,0	25,0	– 1,2	– 6,7	– 10,3
5 mm	– 15,0	25,0	– 1,0	– 6,0	– 10,8
4 mm	– 15,0	25,0	0,3	– 3,7	– 10,9
3,2 mm	– 15,0	25,0	0,2	– 2,4	– 9,5
2,5 mm	– 15,0	25,0	1,3	– 2,6	– 9,5
2 mm	– 15,0	25,0	3,1	– 2,5	– 9,5
1,6 mm	– 15,0	25,0	3,1	– 2,5	– 9,5
1,2 mm	– 15,0	25,0	3,1	– 2,5	– 9,5
1 mm	– 15,0	25,0	3,1	– 2,5	– 9,5
0,8 mm	– 15,0	25,0	3,1	– 2,5	– 9,5

Figure 6.4: Vehicle roughness coefficients table from [13]

Wavelength	$A_{3,i}$						
	Min	Max	Axle load 50 kN — wheel diameter 360 mm	Axle load 50 kN — wheel diameter 680 mm	Axle load 25 kN — wheel diameter 920 mm	Axle load 50 kN — wheel diameter 920 mm	Axle load 100 kN — wheel diameter 920 mm
1 000 mm	– 30,0	0,0	0,0	0,0	0,0	0,0	0,0
800 mm	– 30,0	0,0	0,0	0,0	0,0	0,0	0,0
630 mm	– 30,0	0,0	0,0	0,0	0,0	0,0	0,0
500 mm	– 30,0	0,0	0,0	0,0	0,0	0,0	0,0
400 mm	– 30,0	0,0	0,0	0,0	0,0	0,0	0,0
315 mm	– 30,0	0,0	0,0	0,0	0,0	0,0	0,0
250 mm	– 30,0	0,0	0,0	0,0	0,0	0,0	0,0
200 mm	– 30,0	0,0	0,0	0,0	0,0	0,0	0,0
160 mm	– 30,0	0,0	0,0	0,0	0,0	0,0	0,0
120 mm	– 30,0	0,0	0,0	0,0	0,0	0,0	0,0
100 mm	– 30,0	0,0	0,0	0,0	0,0	0,0	0,0
80 mm	– 30,0	0,0	0,0	0,0	0,0	– 0,2	– 0,2
63 mm	– 30,0	0,0	0,0	– 0,2	– 0,2	– 0,5	– 0,6
50 mm	– 30,0	0,0	– 0,2	– 0,4	– 0,5	– 0,9	– 1,3
40 mm	– 30,0	0,0	– 0,5	– 0,7	– 0,9	– 1,6	– 2,2
31,5 mm	– 30,0	0,0	– 1,2	– 1,5	– 1,6	– 2,5	– 3,7
25 mm	– 30,0	0,0	– 2,0	– 2,8	– 2,5	– 3,8	– 5,8
20 mm	– 30,0	0,0	– 3,0	– 4,5	– 3,8	– 5,8	– 9,0
16 mm	– 30,0	0,0	– 4,3	– 7,0	– 5,8	– 8,5	– 11,5
12 mm	– 30,0	0,0	– 6,0	– 10,3	– 8,5	– 11,4	– 12,5
10 mm	– 30,0	0,0	– 8,4	– 12,0	– 12,0	– 12,0	– 12,0
8 mm	– 30,0	0,0	– 12,0	– 12,5	– 12,6	– 13,5	– 14,0
6,3 mm	– 30,0	0,0	– 11,5	– 13,5	– 13,5	– 14,5	– 15,0
5 mm	– 30,0	0,0	– 12,5	– 16,0	– 14,5	– 16,0	– 17,0
4 mm	– 30,0	0,0	– 13,9	– 16,0	– 16,0	– 16,5	– 18,4
3,2 mm	– 30,0	0,0	– 14,7	– 16,5	– 16,5	– 17,7	– 19,5
2,5 mm	– 30,0	0,0	– 15,6	– 17,0	– 17,7	– 18,6	– 20,5
2 mm	– 30,0	0,0	– 16,6	– 18,0	– 18,6	– 19,6	– 21,5
1,6 mm	– 30,0	0,0	– 17,6	– 19,0	– 19,6	– 20,6	– 22,4
1,2 mm	– 30,0	0,0	– 18,6	– 20,2	– 20,6	– 21,6	– 23,5
1 mm	– 30,0	0,0	– 19,6	– 21,2	– 21,6	– 22,6	– 24,5
0,8 mm	– 30,0	0,0	– 20,6	– 22,2	– 22,6	– 23,6	– 25,4

Figure 6.5: Contact filter coefficients table from [13]

Frequency	$L_{H,VEH,i}$					
	Min	Max	Wheel with diameter 920 mm, no measure	Wheel with diameter 840 mm, no measure	Wheel with diameter 680 mm, no measure	Wheel with diameter 1 200 mm, no measure
50 Hz	60,0	140,0	75,4	75,4	75,4	75,4
63 Hz	60,0	140,0	77,3	77,3	77,3	77,3
80 Hz	60,0	140,0	81,1	81,1	81,1	81,1
100 Hz	60,0	140,0	84,1	84,1	84,1	84,1
125 Hz	60,0	140,0	83,3	82,8	82,8	82,8
160 Hz	60,0	140,0	84,3	83,3	83,3	83,3
200 Hz	60,0	140,0	86,0	84,1	83,9	84,5
250 Hz	60,0	140,0	90,1	86,9	86,3	90,4
316 Hz	60,0	140,0	89,8	87,9	88,0	90,4
400 Hz	60,0	140,0	89,0	89,9	92,2	89,9
500 Hz	60,0	140,0	88,8	90,9	93,9	90,1
630 Hz	60,0	140,0	90,4	91,5	92,5	91,3
800 Hz	60,0	140,0	92,4	91,5	90,9	91,5
1 000 Hz	60,0	140,0	94,9	93,0	90,4	93,6
1 250 Hz	60,0	140,0	100,4	98,7	93,2	100,5
1 600 Hz	60,0	140,0	104,6	101,6	93,5	104,6
2 000 Hz	60,0	140,0	109,6	107,6	99,6	115,6
2 500 Hz	60,0	140,0	114,9	111,9	104,9	115,9
3 160 Hz	60,0	140,0	115,0	114,5	108,0	116,0
4 000 Hz	60,0	140,0	115,0	114,5	111,0	116,0
5 000 Hz	60,0	140,0	115,5	115,0	111,5	116,5
6 350 Hz	60,0	140,0	115,6	115,1	111,6	116,6
8 000 Hz	60,0	140,0	116,0	115,5	112,0	117,0
10 000 Hz	60,0	140,0	116,7	116,2	112,7	117,7

Figure 6.6: Vehicle transfer function table from [13]

Frequency	$L_{H,TR,i}$								
	Min	Max	Mono-block sleeper on soft rail pad	Mono-block sleeper on medium stiffness rail pad	Mono-block on hard rail pad	Bi-block sleeper on soft rail pad	Bi-block sleeper on medium stiffness rail pad	Bi-block sleeper on hard rail pad	Wooden sleepers
50 Hz	0,0	140,0	53,3	50,9	50,1	50,9	50,0	49,8	44,0
63 Hz	0,0	140,0	59,3	57,8	57,2	56,6	56,1	55,9	51,0
80 Hz	0,0	140,0	67,2	66,5	66,3	64,3	64,1	64,0	59,9
100 Hz	0,0	140,0	75,9	76,8	77,2	72,3	72,5	72,5	70,8
125 Hz	0,0	140,0	79,2	80,9	81,6	75,4	75,8	75,9	75,1
160 Hz	0,0	140,0	81,8	83,3	84,0	78,5	79,1	79,4	76,9
200 Hz	0,0	140,0	84,2	85,8	86,5	81,8	83,6	84,4	77,2
250 Hz	0,0	140,0	88,6	90,0	90,7	86,6	88,7	89,7	80,9
316 Hz	0,0	140,0	91,0	91,6	92,1	89,1	89,6	90,2	85,3
400 Hz	0,0	140,0	94,5	93,9	94,3	91,9	89,7	90,2	92,5
500 Hz	0,0	140,0	97,0	95,6	95,8	94,5	90,6	90,8	97,0
630 Hz	0,0	140,0	99,2	97,4	97,0	97,5	93,8	93,1	98,7
800 Hz	0,0	140,0	104,0	101,7	100,3	104,0	100,6	97,9	102,8
1 000 Hz	0,0	140,0	107,1	104,4	102,5	107,9	104,7	101,1	105,4
1 250 Hz	0,0	140,0	108,3	106,0	104,2	108,9	106,3	103,4	106,5
1 600 Hz	0,0	140,0	108,5	106,8	105,4	108,8	107,1	105,4	106,4
2 000 Hz	0,0	140,0	109,7	108,3	107,1	109,8	108,8	107,7	107,5
2 500 Hz	0,0	140,0	110,0	108,9	107,9	110,2	109,3	108,5	108,1
3 160 Hz	0,0	140,0	110,0	109,1	108,2	110,1	109,4	108,7	108,4
4 000 Hz	0,0	140,0	110,0	109,4	108,7	110,1	109,7	109,1	108,7
5 000 Hz	0,0	140,0	110,3	109,9	109,4	110,3	110,0	109,6	109,1
6 350 Hz	0,0	140,0	110,0	109,9	109,7	109,9	109,8	109,6	109,1
8 000 Hz	0,0	140,0	110,1	110,3	110,4	110,0	110,0	109,9	109,5
10 000 Hz	0,0	140,0	110,6	111,0	111,4	110,4	110,5	110,6	110,2

Figure 6.7: Track transfer function table from [13]

Frequency	$L_{W,0,idling}$													
	Min		Max		Diesel locomotive (c. 800 kW)		Diesel locomotive (c. 2 200 kW)		Diesel multiple unit		Electric locomotive		Electric multiple unit	
	SourceA	SourceB	SourceA	SourceB	SourceA	SourceB	SourceA	SourceB	SourceA	SourceB	SourceA	SourceB	SourceA	SourceB
50 Hz	0,0	0,0	140,0	140,0	98,9	103,2	99,4	103,7	82,6	86,9	87,9	92,2	80,5	84,8
63 Hz	0,0	0,0	140,0	140,0	94,8	100,0	107,3	112,5	82,5	87,7	90,8	96,0	81,4	86,6
80 Hz	0,0	0,0	140,0	140,0	92,6	95,5	103,1	106,0	89,3	92,2	91,6	94,5	80,5	83,4
100 Hz	0,0	0,0	140,0	140,0	94,6	94,0	102,1	101,5	90,3	89,7	94,6	94,0	82,2	81,6
125 Hz	0,0	0,0	140,0	140,0	92,8	93,3	99,3	99,8	93,5	94,0	94,8	95,3	80,0	80,5
160 Hz	0,0	0,0	140,0	140,0	92,8	93,6	99,3	100,1	99,5	100,3	96,8	97,6	79,7	80,5
200 Hz	0,0	0,0	140,0	140,0	93,0	92,9	99,5	99,4	98,7	98,6	104,0	103,9	79,6	79,5
250 Hz	0,0	0,0	140,0	140,0	94,8	92,7	101,3	99,2	95,5	93,4	100,8	98,7	96,4	94,3
316 Hz	0,0	0,0	140,0	140,0	94,6	92,4	101,1	98,9	90,3	88,1	99,6	97,4	80,5	78,3
400 Hz	0,0	0,0	140,0	140,0	95,7	92,8	102,2	99,3	91,4	88,5	101,7	98,8	81,3	78,4
500 Hz	0,0	0,0	140,0	140,0	95,6	92,8	102,1	99,3	91,3	88,5	98,6	95,8	97,2	94,4
630 Hz	0,0	0,0	140,0	140,0	98,6	96,8	101,1	99,3	90,3	88,5	95,6	93,8	79,5	77,7
800 Hz	0,0	0,0	140,0	140,0	95,2	92,7	101,7	99,2	90,9	88,4	95,2	92,7	79,8	77,3
1 000 Hz	0,0	0,0	140,0	140,0	95,1	93,0	101,6	99,5	91,8	89,7	96,1	94,0	86,7	84,6
1 250 Hz	0,0	0,0	140,0	140,0	95,1	92,9	99,3	97,1	92,8	90,6	92,1	89,9	81,7	79,5
1 600 Hz	0,0	0,0	140,0	140,0	94,1	93,1	96,0	95,0	92,8	91,8	89,1	88,1	82,7	81,7
2 000 Hz	0,0	0,0	140,0	140,0	94,1	93,2	93,7	92,8	90,8	89,9	87,1	86,2	80,7	79,8
2 500 Hz	0,0	0,0	140,0	140,0	99,4	98,3	101,9	100,8	88,1	87,0	85,4	84,3	78,0	76,9
3 160 Hz	0,0	0,0	140,0	140,0	92,5	91,5	89,5	88,5	85,2	84,2	83,5	82,5	75,1	74,1
4 000 Hz	0,0	0,0	140,0	140,0	89,5	88,7	87,1	86,3	83,2	82,4	81,5	80,7	72,1	71,3
5 000 Hz	0,0	0,0	140,0	140,0	87,0	86,0	90,5	89,5	81,7	80,7	80,0	79,0	69,6	68,6
6 350 Hz	0,0	0,0	140,0	140,0	84,1	83,4	31,4	30,7	78,8	78,1	78,1	77,4	66,7	66,0
8 000 Hz	0,0	0,0	140,0	140,0	81,5	80,9	81,2	80,6	76,2	75,6	76,5	75,9	64,1	63,5
10 000 Hz	0,0	0,0	140,0	140,0	79,2	78,7	79,6	79,1	73,9	73,4	75,2	74,7	61,8	61,3

Figure 6.8: Sound power level at idle from [13]